THE MEASUREMENT OF OSCILLATOR STRENGTHS IN THE PRESENCE OF RESONANCE SELF-BROADENING

Thesis by

Thomas Mark Bieniewski

In Partial Fulfillment of the Requirements

For the Degree of

Doctor of Philosophy

California Institute of Technology

Pasadena, California

1965

(Submitted May 19, 1965)

ACKNOWLEDGEMENTS

This investigation is part of a comprehensive research program on f-values which is being carried out under the direction of Dr. Robert B. King. It is a pleasure to acknowledge his generous help and encouragement on many occasions and in particular, in the preparation of this thesis.

The author also expresses his gratitude to the ARCS Foundation for a fellowship during the year 1959-1960 and to the Cole Foundation for a fellowship during the year 1960-1961.

ABSTRACT

The absolute oscillator strengths for the silver resonance lines, Ag I λλ 3281 and 3383, and the cadmium intersystem line, Cd I λ 3261, were measured from the total absorption for both weak lines and strong lines. For strong lines, cross sections for self-broadening were measured for the resonance lines of silver, lead, thallium, cadmium, and zinc. In the limit of large oscillator strengths, good agreement has been obtained with theory, while for small oscillator strengths, only qualitative agreement has been found.

TABLE OF CONTENTS

TABLE OF CONTENTS
(Continued)

LIST OF TABLES

LIST OF FIGURES

INTRODUCTION

When radiation from a continuous source passes through a gas of free atoms, selective attenuation occurs at those frequencies capable of exciting the atoms to some higher state. An examination of an absorption line thus formed would reveal that it has been dispersed and is no longer infinitely narrow. This dispersion is commonly referred to as "line broadening". Aside from purely instrumental causes and in the absence of external electric or magnetic fields, line broadening can be attributed to the finite lifetimes of the atomic levels involved, to the thermal motions of the absorbers, and to any collisional processes that perturb the atomic levels of the absorber.

Collision broadening can be further delineated by the type of interaction governing the collision. For charged perturbers, Stark broadening occurs which depends on the inverse square of the perturber -- absorber distance in the Linear Start Effect and on the inverse fourth power of this distance in the Quadratic Stark Effect. Next in order of importance comes resonance self-broadening which occurs when the absorber and perturber are both the same kind of atom. The effect of this type of broadening is proportional to the inverse cube of the perturber-absorber separation. Finally, collision broadening is also caused by the Van der Waals forces of other atoms present near the absorber. Since the Van der Waals interaction varies as the inverse sixth power of the absorber-perturber distance, the broadening due to this cause is important only at pressures greater than one atmosphere. As can be seen from this short listing, line broadening encompasses an extensive field. An investigation of this size could not possibly cover the entire field. For more

extensive coverage of line broadening, the reader is referred to the rather substantial literature on the subject [1] .

The interest of this investigation in collision broadening stems from the possibility of using collision broadening as a new means of measuring oscillator strengths. A survey of the various theories of collision broadening reveals that resonance self-broadening varies linearly with the quantity $Nf\lambda$, where N is the atomic density, f is the oscillator strength, and λ is the central wavelength of the unperturbed atomic transition. This particular type of collision broadening could, therefore, be used to measure oscillator strengths, provided that a reliable method be devised for measuring or calculating the cross section for self-broadening.

At present no reliably confirmed theory exists from which cross sections for self-broadening can be calculated. All the present theories [1, 2, 3, 4] predict the same order of magnitude, but differ in the exact numerical value they predict for the cross section. In view of this situation, no attempt was made to calculate the cross sections from any theory. Rather in this investigation the self-broadening cross section was treated as an empirical parameter to be evaluated from the data.

In looking for a method to measure self-broadening cross sections, various methods that had already been used for measuring oscillator strengths were re-examined for their adaptability to this particular experiment. Of the various possibilities considered, only two methods offered real promise; namely, the Hook Method of Rozhdestwensky [5] and the method of total absorption used by King and Stockbarger [6] and by Estabrook [7] . The Hook Method utilizes the anomalous

dispersion near a strong absorption line to measure the oscillator strength. It could be used together with a measurement of the total absorption to yield the cross section for self-broadening. Although the Hook Method is the more accurate of the two methods, the use of a Jamin interferometer over long distances renders it difficult to apply. The method of total absorption was, therefore, chosen for this work.

In this method, a quartz cell is evacuated to a high vacuum ($<10^{-7}$ mm. of Hg), filled with a metallic charge, and sealed under vacuum. The cell is placed in a muffle furnace and is heated to vaporize the metallic sample. The temperature of the cell is carefully measured, and the uniformity of the temperature along the length of the cell is ascertained. After the temperature measurement, the cell with the metallic vapor is irradiated by a source of continuous radiation. The resulting absorption line is dispersed by a 21 foot concave grating spectrograph and photographed on fine grain, high contrast plates. When the plates are developed, the absorption lines are reduced to equivalent widths W_λ by the standard techniques of photographic photometry. Using the temperature measurements, the atomic density can be determined from published vapor pressure data. A plot of W_λ^2/N versus N is next made, and the resulting linear slope yields the cross section for resonance self-broadening.

To summarize then, the primary objective of this investigation is to adapt the method of total absorption to measure resonance self-broadening cross sections for strong lines. Measurements will be made over a wide range of atomic densities and oscillator strengths, and for a number of different spectral transitions. It is hoped that such measurements will

serve to broaden present knowledge about resonance self-broadening, and perhaps even to confirm one of the present theories on the subject. Lastly as an additional objective, this investigation seeks to measure the oscillator strengths for Cd I λ3261 and Ag I $\lambda\lambda$3281 and 3383.

I. THEORETICAL AND EXPERIMENTAL PARAMETERS

Before evaluating any experimental results, it would be well to review the theory of line formation. The purpose for such a resume is to show what parameters the theory predicts for a spectral line and to relate these parameters to the experimentally-measured quantities. First it will be necessary to define the basic terms and mathematical conventions used throughout this work since the usages of various authors differ widely.

In this investigation, ν in sec.$^{-1}$ will denote the frequency, and λ in cm., the wavelength of a spectral line. Also the angular frequency $\omega = 2\pi\nu$ will often be used. To avoid possible confusion between the two types of frequencies, all angular frequencies will always be denoted as (ang. sec.)$^{-1}$. According to this notation, the energy E_{mn} for the transition n→m will be written as $E_{mn} = h\nu_{mn} = \hbar\omega_{mn}$. The order of subscripts, m and n, will always be such that the first subscript refers to the final state and the last subscript to the initial one. Also ν_{mn} is positive for absorption and negative for emission.

Absorption Coefficient

The next parameter to be considered is the absorption coefficient k_ν that characterizes the attenuation of radiation of frequency ν as it traverses an absorbing medium. For a traversal of length $d\ell$ and unit cross section (1cm^2), the decrement of intensity dI_ν determines the absorption coefficient according to the law

$$dI_\nu = -k_\nu I_\nu \, d\ell \tag{I-1}$$

In I-1, I_ν is the intensity in the interval between ν and $\nu + d\nu$ expressed in (ergs sec^{-1} cm^{-2}) $sterad^{-1}$ sec^{+1}. In most cases of practical interest, k_ν does not depend on the path length. A simple integration then yields

$$I_\nu = I_{o\nu} e^{-k_\nu \ell} \tag{I-2}$$

I_ν is called the transmitted intensity, and $I_{o\nu}$, the incident intensity. The simultaneous measurement of both these intensities determines k_ν.

The Residual Intensity and the Equivalent Width

In most experimental situations, I_ν and $I_{o\nu}$ are not accessible to direct measurement. What is usually measured is either the residual intensity of a line:

$$r_\nu = \frac{I_\nu}{I_{o\nu}} = e^{-k_\nu \ell} \tag{I-3}$$

or the equivalent width:

$$W_\nu = \int_0^\infty (1 - r_\nu) \, d\nu = \int_0^\infty (1 - e^{-k_\nu \ell}) \, d\nu \tag{I-4}$$

For an absorption line, r_ν would be found by measuring the depth of the line profile below the continuum, while W_ν would equal the entire area under the line profile. Either measurement permits the evaluation of the absorption coefficient.

Correlation of k_ν with the Oscillator Strength f

After defining the basic terms used in this work, the next task is to relate the absorption coefficient to the oscillator strength. Although there are several approaches that lead to this result, a suitable derivation can be gotten from the condition for monochromatic thermal radiative equilibrium. The equation relating the Einstein A and B coefficients that states this condition is

$$B_{mn} N_n U_\nu = B_{nm} N_m U_\nu + A_{nm} N_m \qquad \text{(I-5)}$$

N_n and N_m are the population densities (in cm^{-3}) of the ground state n and excited state m, respectively, and U_ν is the energy density in the interval between ν and $\nu + d\nu$ in (ergs cm^{-3}) sec. The term on the left in I-5 is the absorption rate, while the terms on the right are the induced emission rate and the spontaneous emission rate, in that order. Since thermal equilibrium has been assumed,

1.) $$\frac{N_m}{N_n} = \frac{g_m}{g_n} e^{-\frac{E_{mn}}{kT}} \qquad \text{(I-6a)}$$

2.) $$U_\nu = \frac{8\pi h\nu^3}{c^3}\left(e^{-\frac{E}{kT}} - 1\right)^{-1} \qquad \text{(I-6b)}$$

The insertion of equations I-6 into I-5 yields two important relations between the Einstein A and B coefficients:

1.) $$g_m B_{nm} = g_n B_{mn} \qquad \text{(I-7a)}$$

2.) $$A_{nm} = \frac{8\pi h \nu_{mn}^3}{c^3}\left(\frac{g_n}{g_m}\right) B_{mn} \qquad \text{(I-7b)}$$

where g is the statistical weight of the state. Equations I-7 show that emission and absorption both depend on the same parameter.

This parameter can be found by considering the rate at which energy is absorbed from an isotropic beam of intensity $4\pi I_\nu = cU_\nu$. From I-1, this rate is seen to be

$$4\pi \int_0^\infty I_\nu k_\nu \, d\nu = cU_\nu \int_0^\infty k_\nu \, d\nu \qquad \text{(I-8)}$$

while equation I-5 gives a rate of

$$h\nu_{mn} B_{mn} N_n U_{\nu_{mn}} \qquad \text{(I-9)}$$

In I-8, U_ν was removed from the integration under the assumption that it varied very little over the line. Equating I-8 and I-9, one has

$$\int_0^\infty k_\nu d\nu = \frac{h\nu_{mn}}{c} B_{mn} N_n \qquad \text{(I-10)}$$

The corresponding classical result is given by Unsold [8] as

$$\int_0^\infty k_\nu d\nu = \frac{\pi e^2}{mc} \eta \qquad \text{(I-11)}$$

where η is the density of classical oscillators. η can be found by considering the definition [9] of the oscillator strength for absorption, f_{mn}: the number of classical oscillators whose absorbing action equals that of a single atom in the given line. Clearly, $\eta = f_{mn} N_n$. A comparison of I-10 and I-11 now yields the desired relation between the absorption

coefficient and the oscillator strength:

$$\int_0^\infty k_\nu \, d\nu = \frac{\pi e^2}{mc} N_n f_{mn} \tag{I-12a}$$

and

$$B_{mn} = \frac{\pi e^2 f_{mn}}{m h \nu_{mn}} \tag{I-12b}$$

I-12b can be combined with I-7b to give

$$A_{nm} = \frac{8\pi^2 e^2 \nu_{mn}^2}{mc^3} \left(\frac{g_n}{g_m} \right) f_{mn} \tag{I-13}$$

Equations I-12b and I13 together demonstrate what has previously been stated; namely, that the strength of both emission and absorption depends on one and the same parameter f_{mn}. The oscillator strength for emission f_{nm} is given by

$$f_{nm} = \left(\frac{g_n}{g_m} \right) f_{mn} \tag{I-14}$$

Up to now, the oscillator strength has been given only a classical interpretation, whereas it does possess an equally important quantum mechanical one. To arrive at the quantum mechanical interpretation, one must first express the transition probability A_{nm} in terms of the matrix elements for the transition m→n. Bethe and Salpeter [10] give this relationship:

$$A_{nm} = \frac{8\pi^2 e^2 \nu_{mn}^2}{mc^3} \left(\frac{4\pi m \nu_{mn}}{3\hbar} \sum_{m_n m_m} \frac{\left| \langle n j_n m_n | \mathbf{r} | m j_m m_m \rangle \right|^2}{2j_m + 1} \right) \tag{I-15}$$

where $\langle n j_n m_n | \mathbf{r} | m j_m m_m \rangle$ are the matrix elements of the dipole operator $\mathbf{r}$. These matrix elements were obtained through the use of the dipole approximation, and represent the expectation value of the dipole moment of the radiating atom. A comparison of I-15 with I-13 now shows that

$$\frac{g_n}{g_m} f_{mn} = f_{nm} = \frac{4\pi m \nu_{mn}}{3\hbar} \sum_{m_n m_m} \frac{\left| \langle n j_n m_n | \mathbf{r} | m j_m m_m \rangle \right|^2}{2 j_m + 1} \qquad \text{(I-16)}$$

In the dipole approximation, therefore, the oscillator strength is determined by the square of the charge distribution of the radiating atom.

II. THEORY

The foregoing section has dealt with the basic theoretical and experimental parameters, and in particular with the quantity of fundamental importance to this investigation, the oscillator strength. This section will briefly outline those aspects of the theory of line formation pertinent to this work. The theoretical considerations presented here will demonstrate how the oscillator strength enters into the equation for the absorption coefficient through the various modes of line broadening. Although the primary concern here is with resonance self-broadening, other forms of line broadening will also be considered. Their inclusion here is justified because a spectral line is usually formed under the simultaneous action of all three mechanisms of broadening — Doppler, radiation damping, and collisions. Each of these modes of broadening introduces its own characteristic parameters into the absorption coefficient. In any experimental situation, the capability of distinguishing the dominant broadening mechanism and the parameters it introduces is of considerable importance. Consequently, a complete theory of line formation is indispensable for properly evaluating experimental data.

Doppler Broadening

Of the three forms of line broadening, perhaps the best understood is Doppler broadening. Doppler broadening results from the uncertainty in the frequency introduced by the thermal motions of the absorbing atoms. According to Doppler's Principle, the shift $\Delta\nu$ in the normal frequency ν_o, due to the thermal motion of the atoms, is given by

$$\Delta\nu = \nu_0 \left(\frac{v}{c}\right) \tag{II-1}$$

where v is the velocity of the absorbing atom along the observer's line of sight. Since thermal equilibrium is one of the conditions of this experiment, one can assume a Maxwell-Boltzmann distribution for the absorber velocity v:

$$P(v) = \left(\frac{M}{2\pi RT}\right)^{\frac{1}{2}} e^{-\frac{Mv^2}{2RT}} \tag{II-2}$$

where M is the mass (in grams) of the absorbing atom; T is the temperature in °K of the isothermal cavity enclosing the absorbing atoms; and R is the universal gas constant. P(v) is, of course, the normalized probability of finding the atom with a velocity between v and v + dv. The insertion of II-1 into II-2 leads at once to the probability distribution of frequencies in the line

$$P(\nu) = \frac{c}{\nu_0}\left(\frac{M}{2\pi RT}\right)^{\frac{1}{2}} \exp.\left(-\frac{Mc^2(\nu-\nu_0)^2}{2RT\nu_0^2}\right) \tag{II-3}$$

Aside from a normalization factor, $P(\nu)$ is completely equivalent to the absorption coefficient k_ν, previously defined. From I-12a, this normalization factor is found to be $\frac{\pi e^2}{mc} N_n f_{mn}$. Setting

$$\Delta\nu_D = \frac{\nu_0}{c}\left(\frac{2RT}{M}\right)^{\frac{1}{2}} \tag{II-4}$$

and using the normalization condition I-12a, the absorption coefficient for pure Doppler broadening becomes

$$k_\nu = \frac{\pi^{\frac{1}{2}} e^2 N_n f_{mn}}{\Delta\nu_D mc} \; e^{-\left(\frac{\Delta\nu}{\Delta\nu_D}\right)^2} \qquad \text{(II-5)}$$

The absorption coefficient is thus seen to be a Gaussian distribution characterized by the Doppler width parameter $\Delta\nu_D$. In this experiment, typical values for $\Delta\lambda_D$ (the Doppler width in wavelength units) are:

1.) Cd I λ3261: $T = 475.8°K$, $\Delta\lambda_D = 2.89 \times 10^{-11}$ cm.
2.) Ag I λ3281: $T = 1002.0°K$, $\Delta\lambda_D = 4.30 \times 10^{-11}$ cm. (II-6)
3.) Ag I λ3383: $T = 1002.0°K$, $\Delta\lambda_D = 4.43 \times 10^{-11}$ cm.

These typical values are listed here for a later comparison with the radiation damping widths and collision broadening widths of these same lines.

Radiation Damping

In any actual experiment, Doppler broadening is almost invariably present, even at room temperatures. To diminish its effect, a number of experimental techniques are often employed. For instance, the lamp emitting the spectral line can be operated at cryogenic temperatures to take advantage of the $\sqrt{T}$ dependence of the Doppler width. Another method, applicable to absorption lines, is to irradiate a highly-collimated atomic beam at right angles. The very small velocity component of the atom along the direction of the light beam reduces the Doppler width

considerably. Even when such techniques are employed, the resulting spectral line is still observed to have a residual finite width. This width can be attributed to the damping action of the emission or absorption process, and is properly called the radiation damping width or natural width.

On a purely classical basis, the electromagnetic field theory of Lorentz and Maxwell can provide an explanation of radiation damping. In the following treatment, two important assumptions will be made. The radiating charge is assumed to be a harmonically-bound oscillating dipole $\mathbf{P} = e\mathbf{r}$. Secondly, the velocity of the dipole oscillator is assumed to be small enough to permit the neglect of all relativistic corrections. With these assumptions, one can write the radiation reaction force on an accelerated charge as [11]

$$\mathbf{F}_{rad.} = \frac{2e}{3c^3}\frac{d^3}{dt^3}\mathbf{P} = \frac{2e^2}{3c^3}\dddot{\mathbf{r}} \qquad \text{(II-7)}$$

The equation for the total force acting on the oscillating charge then becomes

$$m\ddot{\mathbf{r}} = -m\omega_o^2\mathbf{r} + \frac{2e^2}{3c^3}\dddot{\mathbf{r}} \qquad \text{(II-8)}$$

where m and ω_o are the mass and angular frequency of the dipole, respectively. Since the motion of the charge was assumed to be harmonic,

$$\dddot{\mathbf{r}} = -\dot{\mathbf{r}}\omega_o^2 \qquad \text{(II-9)}$$

as a first approximation. Setting $\gamma = \frac{2e^2\omega_o^2}{3mc^3}$, one obtains the equation of a damped harmonic oscillator:

$$\ddot{\mathbf{r}} + \gamma\dot{\mathbf{r}} + \omega_o^2\mathbf{r} = 0 \qquad \text{(II-10)}$$

The amplitude of oscillation is, therefore, given by

$$\mathbf{r}(t) = \mathbf{r}_o e^{i\omega_o t - \frac{1}{2}\gamma t} \qquad \text{(II-11)}$$

A Fourier analysis of this amplitude now yields a dispersion relation for the probability distribution of angular frequencies in the line:

$$P(\omega) = \left|\frac{\mathbf{r}(\omega)}{\mathbf{r}_o}\right|^2 = \frac{\gamma}{2\pi}\left[(\omega-\omega_o)^2 + \left(\frac{\gamma}{2}\right)^2\right]^{-1} \qquad \text{(II-12)}$$

where $P(\omega)$ has been normalized to unity. Clearly, classical physics does predict a dispersion of the spectral line due to radiation damping. The constant γ is the radiation damping width previously referred to. It also has one added significance here. By definition, the full range of angular frequencies over which $P(\omega) \geq 0.5$ is the <u>half-value width</u> $\Delta\omega_{\frac{1}{2}}$, and is seen to exactly equal γ. In wavelength units,

$$\Delta\lambda_{\frac{1}{2}} = \frac{\lambda_o^2}{2\pi c}\gamma = \frac{4\pi e^2}{3mc^2} = 1.17 \times 10^{-12}\ \text{cm.} \qquad \text{(II-13)}$$

A comparison of $\Delta\lambda_{\frac{1}{2}}$ with the Doppler widths $\Delta\lambda_D$ observed in this investigation (Equations II-6) reveals that in most experimental situations, γ can be neglected in comparison with $\Delta\omega_D$.

Equation II-13 indicates that the classical radiation damping width, expressed in wavelength units, is a constant independent of the particular optical transition. This prediction completely disagrees with the quantum theory of radiation damping proposed by Weisskopf and Wigner [12] and by Hoyt [13] . This theory predicts that the radiation damping width should vary with the oscillator strength. Fortunately, experiments have completely resolved this disagreement. The subsequent work of many investigators and also this investigation have verified the correctness of the quantum mechanical prediction. Consequently, the usefulness of the classical theory of radiation is severely limited. The classical theory correctly predicts a dispersion relation for the line profile, but the damping widths it predicts can be too large by several orders of magnitude. For quantitative work, one must resort to the quantum mechanical theory.

Since the quantum theory of radiation damping is firmly established, both theoretically and experimentally, this section need present only those portions of it pertinent to this investigation. For a complete theoretical exposition, references [12, 13] should be consulted. Like its classical counterpart, the quantum theory of radiation damping predicts a dispersion equation for the line profile. Normalized to unity, this relation takes the form

$$P(\omega) = \frac{\gamma}{2\pi}\left[(\omega - \omega_0)^2 + \left(\frac{\gamma}{2}\right)^2 \right]^{-1} \qquad \text{(II-14)}$$

where γ is the radiation damping width. In equation II-14, γ is to be found from the quantum mechanically derived expression:

$$\gamma = \frac{8\pi^2 e^2 \nu_{mn}^2}{mc^3} \left\{ \frac{4\pi m \nu_{mn}}{3\hbar} \sum_{m_n m_m} \frac{\left| \langle n j_n m_n | r | m j_m m_m \rangle \right|^2}{2j_m + 1} \right\} \quad \text{(II-15)}$$

Comparison of equation II-15 with I-16 shows that the expression in braces is $(2j_n + 1) f_{mn} / (2j_m + 1)$ where f_{mn} is the oscillator strength for the absorption of radiation from the ground state n to the excited state m. Consequently, the quantum mechanically derived radiation damping width becomes

$$\gamma = A_{nm} = \frac{8\pi^2 e^2 \nu_{mn}^2}{mc^3} \left(\frac{g_n}{g_m} \right) f_{mn} \quad \text{(II-16)}$$

a result identical with that found previously in I-13. Equation II-16 clearly demonstrates that the radiation damping width is independent of the atomic density, N. This result is quite important since it permits a separation of the radiation damping width from the collision broadening width which does depend on the atomic density. Also II-16, contrary to the classical prediction, shows that the radiation damping width does depend on the particular optical transition through the oscillator strength and the statistical weights of the participating atomic levels. This latter result is also of some value to this investigation because it allows one to measure the oscillator strength of a strong line even if the resonance self-broadening cross section is unknown.

Collision Broadening

As the density of atoms increases, collisions begin to have a greater effect on the line shape than radiation damping. For resonance self-broadening, the current theories claim to yield only the correct order of magnitude for the collision cross section. However, there now appears to be at least one theory, due to Einar Lindholm [4] , capable of giving quantitative results. His theory is quite general in that it treats the collision broadening due to an interaction potential

$$V = \frac{C_p}{R^p} \qquad \text{(II-17)}$$

at all atomic densities. The constant C_p is the force constant for the broadening interaction, and R is the separation between the colliding atoms. The exponent p = 3 for resonance self-broadening, and p = 6 for Van der Waals broadening. The one serious drawback to using Lindholm's theory is the need for either a calculated or measured value of the force constant C_p. Later in this section, a value for C_p will be found from a theory recently proposed by H. M. Foley [2] .

The treatment of Lindholm's theory presented here centers around the Correlation Function for an oscillator [14] . One begins by assuming the interaction potential in II-17. For convenience, the classical path approximation is also assumed. That is, each collision will be characterized by a collision parameter ρ which is the distance of closest approach in a collision. With these assumptions, the phase shift caused by a collision is:

$$\eta(\rho) = \frac{1}{\hbar}\int_{-\infty}^{\infty}\frac{C_p\,dt}{\left[\rho^2 + v^2(t-t_o)^2\right]^{p/2}} = \frac{\alpha_p C_p}{\hbar v \rho^{p-1}} \qquad \text{(II-18)}$$

In II-18, v is the average relative velocity between the colliding atoms, and

$$\alpha_p = \frac{\pi^{\frac{1}{2}} \Gamma\left(\frac{p-1}{2}\right)}{\Gamma\left(\frac{p}{2}\right)} \tag{II-19}$$

Under the action of time-varying forces, the amplitude of the oscillator whose natural angular frequency is ω_o will be given by

$$f(t) = e^{i\int_o^t \omega(t')dt'} = e^{i\omega_o t + i\eta(t)} \tag{II-20}$$

$\eta(t)$ is the sum of all the phase shifts in the time interval from 0 to t and can be expressed as

$$\eta(t) = \int_o^t \left[\omega(t') - \omega_o\right] dt' \tag{II-21}$$

One can now introduce the Correlation Function $\phi(s)$:

$$\phi(s) = e^{i\omega_o s} \lim_{T\to\infty} \frac{1}{T} \int_{-\frac{T}{2}}^{\frac{T}{2}} f^*(t) f(t+s)\, d(t) \tag{II-22a}$$

which by using II-20 becomes

$$\phi(s) = \lim_{T\to\infty} \frac{1}{T} \int_{-\frac{T}{2}}^{\frac{T}{2}} e^{i\left[\eta(t+s) - \eta(t)\right]} dt \tag{II-22b}$$

The normalization $\phi(0) = 1$ has been chosen in both equations. $\phi(s)$ represents the degree of correlation in the oscillator's phase before and after a collision. In extremely strong collisions, $\phi(s)$ is very small, indicating a severe disruption in the oscillator's phase, whereas a large value of $\phi(s)$ implies a weak collision that merely produces a small phase shift. The importance of $\phi(s)$ to this problem lies in the fact that the Fourier transform of $e^{i\omega_o s}\phi(s)$ yields $I(\omega)$, the line profile. This relationship can readily be demonstrated:

$$\lim_{S\to\infty} \frac{1}{2\pi}\int_{-S/2}^{S/2} \phi(s)\, e^{i(\omega_o-\omega)s}\, ds =$$

$$\lim_{S\to\infty}\lim_{T\to\infty} \frac{1}{2\pi T}\int_{-T/2}^{T/2} f^*(t)\, e^{i\omega t}\int_{-S/2}^{S/2} f(t+s)\, e^{-i\omega(t+s)}\, ds\, dt \qquad \text{(II-23)}$$

In II-23, the inner integral on the right-hand side cannot depend on t because only the zero-point of the time scale is affected by t. Such a zero-point is meaningless for an infinite time interval. Therefore, changing the integration variable s to t in the right-hand side of II-23, one has

$$\lim_{S\to\infty} \frac{1}{2\pi}\int_{-S/2}^{S/2} \phi(s)\, e^{i(\omega_o-\omega)s}\, ds = I(\omega) =$$

$$\lim_{T\to\infty} \frac{1}{2\pi T}\int_{-T/2}^{T/2} f^*(t)\, e^{i\omega t}\, dt \int_{-T/2}^{T/2} f(t)\, e^{-i\omega t}\, dt \qquad \text{(II-24)}$$

The right-hand side of II-24 can now be identified as the definition of the line profile $I(\omega)$.

To simplify the notation, the quantity $\eta(t + s) - \eta(t)$, occurring in II-22b, will be shortened to

$$\eta(t,s) = \eta(t+s) - \eta(t) \tag{II-25a}$$

and

$$\phi(s) = \lim_{T\to\infty} \frac{1}{T}\int_{-T/2}^{T/2} e^{i\eta(t,s)}dt = \overline{e^{i\eta(t,s)}} \tag{II-25b}$$

The bar over $e^{i\eta(t,\,s)}$ signifies the time average of $e^{i\eta(t,\,s)}$ over the radiation process. If one considers a collision during a time interval ds, then the phase shift η' due to the collision can be found from the relation:

$$e^{i\eta(t,\,s+ds)} - e^{i\eta(t,s)} = e^{i\eta(t,s)}\left(e^{i\eta'} - 1\right) \tag{II-26}$$

Taking the time average of II-26 and using II-25b, one has

$$\phi(s+ds) - \phi(s) = d\phi(s) = \overline{e^{i\eta(t,s)}\left(e^{i\eta'} - 1\right)} \tag{II-27}$$

By definition, η' is the phase shift in the time interval $t + s$ and $t + s + ds$, while $\eta(t, s)$ is the sum of the phase shifts during the interval t and $t + s$. The randomness of the collision process would lead one to expect that η' and $\eta(t, s)$ are independent of each other. Making

this assumption permits one to replace the time average of the product in II-27 by the product of the respective time averages. Mizushima [15] has investigated this approximation and found that it does not affect the validity of the final result. The decomposition of II-27 into the product of time averages yields the differential equation linking η' to $\phi(s)$:

$$d\phi(s) = \phi(s)\overline{(e^{i\eta'} - 1)} \qquad \text{(II-28)}$$

Mathematically, it would be very convenient if the rather intractable time average in II-28 could be replaced by a suitable average over all possible collision parameters p. This replacement can be justified as follows [16] .

From equations II-21 and II-26, η' can be explicitly evaluated as:

$$\eta' = \int_t^{t+ds} \left[\omega(t') - \omega_o \right] dt' \qquad \text{(II-29)}$$

Thus, the time average $\overline{e^{i\eta'}-1}$ becomes:

$$\overline{e^{i\eta'} - 1} = \lim_{T \to \infty} \frac{1}{T} \int_{-T/2}^{T/2} \left\{ e^{i\int_t^{t+ds} [\omega(t') - \omega_o] dt'} - 1 \right\} dt \qquad \text{(II-30)}$$

Clearly, the right-hand side of II-30 is really the sum of $e^{i\eta'}-1$ over all intervals ds in which a collision produces a non-zero phase shift η'. Assuming that there are M such intervals ds, one can associate with each interval a collision parameter p that characterizes the collision in that interval. The random nature of the collision process now

assures the complete randomness in the distribution of collision parameters ρ obtained in this manner for a single oscillator. If one now assumes that there are M independent identical oscillators, each of which suffers a collision during the single interval ds, then the random distribution of collision parameters ρ obtained in this second way should be the same as that obtained for the single oscillator. This, of course, implies that the distribution of phase shifts $\eta'(\rho)$ is the same in both cases. Therefore, one is justified in replacing the time average in II-28 by the weighted average over the collision parameter ρ. The weight function, needed here, is simply the number of atoms per cm.^{3} that in the time interval ds suffer a collision with a collision parameter between ρ and $\rho + d\rho$. From the kinetic theory of gases [17] , the proper weight function is

$$G(\rho; ds) = 2\pi \rho d\rho \cdot N v ds \qquad \text{(II-31)}$$

where N is the atomic density, and v is the relative velocity between the colliding atoms. Using II-31, one finally obtains:

$$\overline{e^{i\eta} - 1} = N v ds \cdot 2\pi \int_0^\infty \left(e^{i\eta(\rho)} - 1\right) \rho d\rho$$

$$= -N v ds \, (\sigma_r - i\sigma_i) \qquad \text{(II-32)}$$

where the prime has been dropped from $\eta(\rho)$. The cross sections σ_r and σ_i are given by the integral:

$$\sigma = \sigma_r - i\sigma_i = -2\pi \int_0^\infty \left(e^{i\eta(\rho)} - 1\right) \rho d\rho \qquad \text{(II-33)}$$

Inserting the result II-32 into II-28, one obtains

$$\phi(S) = e^{-Nv(\sigma_r - i\sigma_i)S} \tag{II-34}$$

which by II-24 leads to the line profile

$$I(\omega) = \frac{Nv\sigma_r}{\pi}\left[(\omega - \omega_o - Nv\sigma_i)^2 + (Nv\sigma_r)^2\right]^{-1} \tag{II-35}$$

Thus, the real part of the total cross section σ is σ_r, the cross section for line broadening, while the imaginary part σ_i is the cross section for shifting the central wavelength of the line profile. Equation II-35 shows that in the impact approximation, collision broadening leads to a dispersion relation for the line profile with a half-value width $\gamma_c = 2Nv\sigma_r$. Also the maximum of the line profile has been shifted from ω_o by an amount $\Delta\omega_c = Nv\sigma_i$. Experimentally, it has been shown that resonance self-broadening does not yield a shift in the maximum of line profile, whereas Van der Waals broadening results in a shift whose sign depends on the foreign gas present.

Now that the line profile for collision broadening has been obtained, it would be advantageous to calculate σ_r from some theory in order to compare it later with experimentally-measured values. Such a derivation will be made here from a theory on resonance self-broadening introduced by H. M. Foley [2] . Foley's theory is based also on the impact approximation, and is divided into two limiting cases, depending on the magnitude of the oscillator strength. For large oscillator

strengths, Foley begins with the operator T satisfying the equation

$$i\hbar \dot{T} = \left[U^{-1}(t, t_o) H_c(\rho, t) U(t, t_o) \right] T \qquad \text{(II-36)}$$

where $U(t, t_o)$ is the time development operator corresponding to the Hamiltonian operator H_o for the unperturbed system, and $H_c(\rho, t)$ is the Hamiltonian for a single collision with impact parameter ρ. Taking matrix elements of II-36,

$$i\hbar \langle m| \dot{T} |n\rangle = e^{\frac{i}{\hbar}(E_m - E_n)t} \langle m| H_c(\rho, t) |n\rangle \langle n| T |m\rangle \qquad \text{(II-37)}$$

In the impact approximation, the collision duration is short compared with the radiation lifetime. Thus, the oscillatory factor in II-37 equals unity, and formally

$$T = \exp\left[-\frac{i}{\hbar} \int_{-\infty}^{\infty} H_c(\rho, t) dt \right] \qquad \text{(II-38)}$$

where $H_c(\rho, t)$ is now to be considered as a matrix over the magnetic sublevels of the system; i.e., a $(2J + 1) \times (2J + 1)$ matrix.

For a dipole-dipole interaction, the Hamiltonian, $H_c(\rho, t)$ takes the form

$$H_c(\rho, t) = \frac{(\mathbb{P} \cdot \mathbb{R})(\mathbb{\Pi} \cdot \mathbb{R})}{R^5} - \frac{\mathbb{P} \cdot \mathbb{\Pi}}{R^3} \qquad \text{(II-39)}$$

where the Latin letters refer to one atom and the Greek letters to the other atom, and $\mathbb{P}$ and $\mathbb{\Pi}$ are the electric dipole moments of the

two atoms. Decomposing equation II-39 into cartesian coordinates, one obtains: (refer to Appendix II for a sketch of the coordinate system)

$$H_c(\rho,t) = \frac{3(P_z\pi_\xi - P_y\pi_\eta)\rho^2}{(\rho^2+v^2t^2)^{5/2}} - \frac{3(P_z\pi_\xi - P_x\pi_\xi)\rho vt}{(\rho^2+v^2t^2)^{5/2}}$$

$$+ \frac{(2P_y\pi_\eta - P_x\pi_\xi - P_z\pi_\zeta)}{(\rho^2+v^2t^2)^{3/2}} \qquad \text{(II-40)}$$

Inserting equation II-40 into II-38 and integrating, the first term yields $4/3\rho^2 v$, the second term vanishes, and the third term gives $2/\rho^2 v$. Hence,

$$T = \exp\left[-\frac{2i}{\hbar v\rho^2}\left(P_z\pi_\zeta - P_x\pi_\xi\right)\right] \qquad \text{(II-41)}$$

The matrix T must now be evaluated using eigenfunctions symmetric (or anti-symmetric) in the two atoms. To simplify the calculation, the ground state ϕ_g° and the upper state ϕ_e^m will be assumed to have J = 0 and J = 1, respectively. This assumption limits the rank of the matrix to be diagonalized to rank three. Thus,

$$M_1^{mm'} = \frac{1}{2}\left\langle \phi_g^\circ(1)\,\phi_e^m(2) + \phi_e^m(1)\,\phi_g^\circ(2)\middle| P_z\pi_\zeta - P_x\pi_\xi \middle| \phi_g^\circ(1)\,\phi_e^{m'}(2) + \phi_e^{m'}(1)\,\phi_g^\circ(2)\right\rangle \qquad \text{(II-42)}$$

where the numbers 1 and 2 refer to the spatial coordinates of atoms 1 and 2, respectively. Equation II-42 reduces to

$$M_1^{mm'} = \left\langle \phi_g^\circ(1)\middle| P_z \middle| \phi_e^{m'}(1)\right\rangle\left\langle \phi_e^m(2)\middle| \pi_\zeta \middle| \phi_g^\circ(2)\right\rangle$$
$$- \left\langle \phi_g^\circ(1)\middle| P_x \middle| \phi_e^{m'}(1)\right\rangle\left\langle \phi_e^m(2)\middle| \pi_\xi \middle| \phi_g^\circ(2)\right\rangle \qquad \text{(II-43)}$$

Evaluating II-43 in terms of reduced matrix elements [18] ,

$$M_1^{mm'} = |\langle g \| \mathbb{P} \| e \rangle|^2 \begin{bmatrix} -\frac{1}{2} & 0 & \frac{1}{2} \\ 0 & 1 & 0 \\ \frac{1}{2} & 0 & -\frac{1}{2} \end{bmatrix} \tag{II-44}$$

where m and m' decrease from the upper left corner. Hence

$$T = \exp. \left\{ \frac{-2i}{\hbar v \rho^2} |\langle g \| \mathbb{P} \| e \rangle|^2 \begin{bmatrix} -\frac{1}{2} & 0 & \frac{1}{2} \\ 0 & 1 & 0 \\ \frac{1}{2} & 0 & -\frac{1}{2} \end{bmatrix} \right\} \tag{II-45a}$$

$$T = \exp. \left\{ i \begin{bmatrix} a & 0 & c \\ 0 & b & 0 \\ c & 0 & a \end{bmatrix} \right\} \tag{II-45b}$$

where $a = \alpha/\rho^2$, $b = -2\alpha/\rho^2$, $c = -\alpha/\rho^2$, and $\alpha = |\langle g \| \mathbb{P} \| e \rangle|^2 / \hbar v$.

The matrix in equation II-45b can be diagonalized by a matrix S, given by

$$\begin{bmatrix} b & 0 & 0 \\ 0 & (a+c) & 0 \\ 0 & 0 & (a-c) \end{bmatrix} = \begin{bmatrix} 0 & 1/\sqrt{2} & 1/\sqrt{2} \\ 1 & 0 & 0 \\ 0 & 1/\sqrt{2} & -1/\sqrt{2} \end{bmatrix}^{-1} \begin{bmatrix} a & 0 & c \\ 0 & b & 0 \\ c & 0 & a \end{bmatrix} \begin{bmatrix} 0 & 1/\sqrt{2} & 1/\sqrt{2} \\ 1 & 0 & 0 \\ 0 & 1/\sqrt{2} & -1/\sqrt{2} \end{bmatrix} \tag{II-46}$$

Using the matrix S, T becomes

$$T = S \begin{bmatrix} e^{ib} & 0 & 0 \\ 0 & e^{i(a+c)} & 0 \\ 0 & 0 & e^{i(a-c)} \end{bmatrix} S^{-1} \tag{II-47}$$

The cross section for resonance self-broadening can now be evaluated using the relation:

$$\sigma_r = \text{Real}\left\{ 2\pi \int_0^\infty \left[1 - \tfrac{1}{3}\left(e^{ib} + e^{i(a+c)} + e^{i(a-c)} \right) \right] \rho \, d\rho \right\} \qquad \text{(II-48)}$$

Inserting the definitions of a, b, and c, yields the integral

$$\sigma_r = \frac{8\pi}{3} \int_0^\infty \sin^2\left(\frac{\alpha}{\rho^2}\right) \rho \, d\rho \qquad \text{(II-49)}$$

No angular average of the integral in II-49 over the Euler angles will be needed because of the isotropy of space. The indicated integration is readily performed to yield

$$\sigma_r = \frac{\pi r_0 c \lambda f_e}{6v} \qquad \text{(II-50)}$$

where λ and fe refer to the resonant transition to the ground state. Thus, fe is an oscillator strength for emission. Since oscillator strengths for absorption are used exclusively throughout this investigation, equation II-50 can be rewritten:

$$\sigma_r = \frac{\pi r_0 c \lambda}{6v} \left(\frac{g_l}{g_u} \right) f_a \qquad \text{(II-51)}$$

where g_l and g_u are the statistical weights of the lower and upper levels, respectively. Equation II-51 will later be compared with experimentally measured cross sections. To facilitate such a comparison,

equation II-51 can be refactored into the form:

$$\epsilon = \frac{2 g_u V \sigma_r}{g_\ell \lambda f_a} = \frac{\pi}{3} r_o c = 8.85 \times 10^{-3} \text{ cm}^2/\text{sec.} \quad \text{(II-52)}$$

where r_o is the classical electron radius and c is the velocity of light. The reduced cross section ϵ will actually be the quantity later compared with the experimental measurements of this investigation.

For oscillator strengths much less than 0.1, equation II-50 no longer correctly describes the resonance self-broadening cross section. As the oscillator strength decreases, the first order matrix elements of the Hamiltonian $H_c(\rho, t)$ become very small. If as Foley predicts, the second order contribution from $H_c(\rho, t)$ does not depend on the oscillator strength, then conceivably for sufficiently small oscillator strengths, the second order terms could exceed the first order contribution from $H_c(\rho, t)$. In that event, the perturber would act more like a foreign gas atom. One would expect that in the impact approximation, the collision damping width would be linearly proportional to the atomic density and would have a velocity dependence. Unfortunately, it is not clear from Foley's article whether his predictions of the self-broadening cross sections for the zinc and cadmium intersystem lines are directly comparable to the measurements reported here. Measurements obtained in this investigation were made in the absence of an external magnetic field (<10 gauss) and represent the average self-broadening seen by <u>all</u> the magnetic sublevels of the upper state. Foley's predictions, on the other hand, were meant to be applied to the self-broadening of the

$m = 0 \rightarrow m = 1$ transition of the upper state in the presence of an external magnetic field. For this reason no direct comparison will be made between the cadmium and zinc cross sections measured here and the corresponding predictions in Foley's article.

The Effect of Line Broadening on the Equivalent Width

Previous discussion of line broadening has centered around its effect on the line profile and the closely-related quantity, the absorption coefficient. Equation I-4 shows that the equivalent width W_ν depends on the absorption coefficient. Since the equivalent width W_ν was the quantity measured in the experiments reported here, the effect of line broadening on W_ν should be investigated. To determine this effect, the form of the absorption coefficient k_ν must be known when more than one type of line broadening is present. If a spectral line is being broadened by both radiation damping and collisions, the resulting line profile $I(\omega)$ is given by the convolution integral of II-14 and II-35:

$$I(\omega) = \frac{\gamma_N \gamma_c}{4\pi^2} \int_{-\infty}^{\infty} \left[\frac{1}{(\omega' - \omega_0)^2 + (\gamma_c/2)^2}\right]\left[\frac{1}{(\omega' + \omega - \omega_0)^2 + (\gamma_N/2)^2}\right] d\omega' \qquad \text{(II-53)}$$

Carrying out the integration in II-53 gives:

$$I(\omega) = \frac{\gamma}{2\pi}\left[(\omega - \omega_0)^2 + (\gamma/2)^2\right]^{-1} \qquad \text{(II-54a)}$$

where $\gamma = \gamma_N + \gamma_c$, and

$$k_\nu = \frac{r_0 c}{4\pi} N f \gamma \left[(\nu - \nu_0)^2 + (\gamma/4\pi)^2\right] \qquad \text{(II-54b)}$$

If Van der Waals broadening is also present, then its Lorentzian line profile must be folded with that in Equation II-54a. The resulting convolution integral yields a dispersion relation with $\gamma = \gamma_N + \gamma_c + \gamma_W$, γ_W being the Van der Waals damping width. Equation II-54b was obtained by multiplying II-54a by the normalization $\pi r_o cNf$ and converting to pure frequency units. Thus, the simultaneous presence of radiation damping and collision broadening leads to the dispersion relation in II-54b for the absorption coefficient k_ν. To include the effect of Doppler broadening on the absorption coefficient, the convolution integral of II-3 and II-54b is needed:

$$k_\nu = \frac{r_o c N f}{\pi^{1/2}} \left(\frac{\gamma}{4\pi \Delta\nu_D} \right) \int_{-\infty}^{\infty} \frac{e^{-\left(\frac{\Delta\nu'}{\Delta\nu_D}\right)^2} d(\Delta\nu')}{(\nu - \nu_o - \Delta\nu')^2 + (\gamma/4\pi)^2} \qquad \text{(II-55)}$$

The normalization in II-55 corresponds to that given in I-12a. Equation II-55 with $\gamma = \gamma_N + \gamma_W + \gamma_c$ represents the absorption coefficient of a line simultaneously broadened by the Doppler Effect, radiation damping, and collisions.

Of special significance is the quantity $a = \gamma/4\pi\Delta\nu_D$ occurring in II-55. This quantity is called the damping ratio, and its magnitude determines the shape of the curve of growth. For large values of the damping ratio ($a > 1$), and for equivalent widths W_λ exceeding ten times the Doppler width $\Delta\lambda_D$, the spectral line may be considered strong, and the absorption coefficient in II-55 reduces to II-54b with an error not exceeding 5 per cent. The equivalent width W_λ for a strong line can be found by substituting II-54b into I-4 and integrating:

$$W_\lambda = \frac{\lambda_o^2}{c} W_\nu = \sqrt{\left(\frac{r_o \ell \lambda_o^4}{c}\right) N f_a \gamma} = \sqrt{F N f_a \gamma} \qquad \text{(II-56)}$$

where W_λ is the equivalent width in wavelength units, ℓ is the path length, r_o is the classical electron radius, and λ_o is the central wavelength of the unperturbed transition. For very small values of the damping ratio ($0 < a < 0.01$) and for equivalent widths W_λ not exceeding twice the Doppler width $\Delta\lambda_D$, the spectral line may be considered weak, and the absorption coefficient in II-55 reduces to II-5 with an error not exceeding a few per cent. The equivalent width W_λ for a weak line cannot be evaluated in closed form. However, W_λ can be developed in a series [19]:

$$W_\lambda = \pi^{1/2} \Delta\lambda_D C \sum_{n=1}^{\infty} \frac{(-1)^{n-1} C^{n-1}}{n!\, n^{1/2}} \qquad \text{(II-57a)}$$

where $\Delta\lambda D$ is the Doppler width in wavelength units, and

$$C = \left(\frac{\pi^{1/2} r_o \lambda_o^2}{\Delta\lambda_D}\right) N f_a \ell \qquad \text{(II-57b)}$$

Equations II-56, II-57a, and II-57b are the expressions that were used to calculate the oscillator strength f_a and the half-value width γ from measurements of the atomic density N in atoms /cm^3, the temperature T in ^oK, and the equivalent width W_λ in cm.

For weak lines, equations II-57 were used to compute the oscillator strength f_a. For strong lines, a different procedure was followed.

First, published vapor pressure data and equation II-56 were used to compute $f_a\gamma$ at a series of different temperatures from equivalent widths of strong lines. The resulting values of $f_a\gamma = f_a(\gamma_N + \gamma_W + \gamma_c)$ were then fitted to an equation of the form, $\gamma f_a = A + BN$, by the method of least squares. Upon obtaining the two constants A and B, the reduced cross section for self-broadening ϵ could be found from the relation

$$B = f_a (f_e \lambda \epsilon) \tag{II-58}$$

and in the absence of Van der Waals broadening $\gamma_W = 0$, the oscillator strength f_a could be gotten from the relation

$$A = f_a \gamma_N = \frac{8\pi^2 r_o c}{\lambda^2}\left(\frac{g_\ell}{g_u}\right) f_a^2 \tag{II-59}$$

III. APPARATUS AND EXPERIMENTAL PROCEDURES

Preparation of Absorption Cells

Fused quartz is an ideal material for cells used in ultra-violet absorption spectroscopy. Because fused quartz is amorphous, it can be readily fabricated into complex shapes by standard glass-blowing techniques. Also fused quartz is transparent throughout the ultra-violet and can withstand prolonged use at temperatures up to 1300° C. For these reasons, the absorption cells used in this investigation were made from fused quartz. Absorption cells were fabricated by cutting one inch O. D. quartz tubing into 1. 6 inch long sections. Quartz windows were fused to both ends of a section to contain the vapor and transmit the incident radiation. The resulting cylindrical chamber had a four inch long side-arm fused to the middle of its side. This side-arm consisted of a 1/4 inch glass tube with a quartz-to-pyrex graded seal that permitted fusing the cell to an all-glass vacuum system.

Before fusing a cell to the vacuum system, its interior was cleansed with aqua regia ($3HNO_3$ + HCl) and thoroughly rinsed with triply distilled water. After pumping the cell to dryness, the metallic sample was inserted into a quartz distillation bulb attached to the cell. The cell was then fused to the vacuum system. The vacuum system consisted of a forepump, an all-glass water-cooled mercury diffusion pump (50 liters/sec pumping speed), three cold traps, and a glass manifold. To prevent condensation of mercury in the manifold, two liquid nitrogen cold traps were located between the manifold and the diffusion pump. The diffusion of forepump oil through the system was

blocked by placing a cold trap immediately after the forepump. These precautions effectively kept all contaminating vapors from the absorption cell. To monitor the pressure, an RCA 1949 glass ionization gauge was fused to the glass manifold.

When the system had pumped down to a pressure of about 10^{-5} mm of Hg., the metallic charge in the distillation bulb was vaporized to remove any adsorbed gases. The cell itself was baked at a 1000° C for at least eight hours to remove any volatile contaminants. Also, the entire vacuum manifold was vigorously heated with an air-gas torch to improve the vacuum. Upon reaching its ultimate vacuum of 10^{-7} mm of Hg., the system was allowed to cool, and the metallic charge in the distillation bulb was distilled directly into the cell. While still under vacuum, the cell was fused shut with an oxyhydrogen torch and pulled free from the glass vacuum manifold. The evacuated cell with its metallic sample was inserted into a furnace and heated to vaporize the metal.

The Vacuum Furnace

This investigation used a furnace made of brass with a cylindrical working space eighteen inches long and eight inches in diameter. A flange on either rim of the cylinder provided space for an O-ring groove and a circle of six bolts. By means of these bolts, a brass end-plate could be bolted to each end of the furnace, thus providing a vacuum-tight seal. To cool the furnace during operation, the cylindrical shell of the furnace and both end-plates were provided with double walls so that tap water could flow through them. The double walls of the furnace were pierced in two places. One opening provided a vacuum outlet to

the forepump. The other opening allowed a Pirani gauge to monitor the pressure in the furnace. To permit radiation to pass through the furnace, each end-plate had a circular aperture at its center with a 2.5 inch diameter. These apertures were covered by three inch quartz discs pressing against O-ring seals. One of the end-plates had six additional openings drilled in it. Three of these held vacuum-tight power leads for the furnace, and the other three holes admitted three thermocouples into the furnace through vacuum-tight neoprene glands.

On the same end-plate with the thermocouple glands and power leads, there were fastened three fifteen inch long brass rods. These rods, spaced 120° apart, provided a frame for supporting the furnace elements without allowing them to touch the furnace walls. This arrangement minimized heat conduction to the furnace walls, while the vacuum in the furnace eliminated heat losses through convection. Alundum spacers separated the furnace elements concentrically from each other. Beginning with the outermost element, the parts of the furnace were: a thin-walled nickel radiation shield (6" I. D.), a thick-walled alundum radiation shield (3.75" O. D., 3" I. D.), and two alundum heating coils one inside the other. The outer heating coil had a two inch diameter and was wound one-third of the way from each end with 0.020 inch molybdenum wire. The inner heating coil had a 1.75 inch diameter and was wound along its entire ten inch length with the same type of wire. The purpose for this particular arrangement of the heating coils is as follows: by heating both ends of the outer coil, the temperature gradient inside the inner coil could be kept uniform over a distance of 2.5 inches

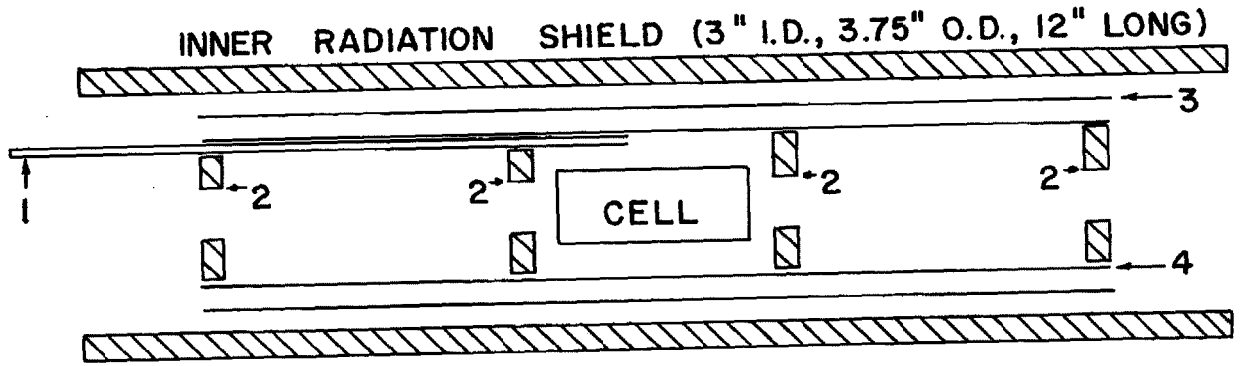

1. THERMOCOUPLE TUBE
2. FURNACE APERTURE
3. OUTER HEATING COIL (2" I.D., 10" LONG)
4. INNER HEATING COIL (1.75" I.D., 10" LONG)

FIGURE 1. SCHEMATIC VIEW OF FURNACE

about the center. Moreover, the temperature gradient at the center of the furnace could be regulated independently of the current heating the inner coil. Before an experiment, the absorption cell was inserted into the center of the furnace. Two alundum discs with 5/8 inch square apertures were placed on either side of the cell, and two more such discs were used to cap the ends of the inner coil. These four discs were notched at three points spaced 120° apart on their rims to permit the insertion and removal of thermocouple tubes.

With the cell in position, the furnace was heated by passing an electric current through the heating coils. The source of power was a 3 KVA Sola constant voltage transformer with a 220 VAC tap and a 110 VAC tap. The inner heating coil was operated through a variac connected to the 220 VAC tap on the Sola transformer. With this arrangement, the current heating the inner coil could be varied continuously from zero to eight amperes, permitting steady state temperatures up to 1450° C. Both ends of the outer heating coil were operated in series through a second variac connected to the 110 VAC tap on the Sola transformer. Generally, it was possible to adjust both variacs until the temperature gradient at the center of the furnace was less than 1° C. Also, each coil had an ammeter in series with it to measure its current.

Temperature Measurements:

Of the measurements taken in this investigation, the temperature measurement was the most critical. Vapor pressures of metals require an accurate knowledge of the temperature because of their steep exponential dependence on temperature. All temperatures were, therefore,

measured with Pt-Pt, 10% Rh thermocouples whose calibration was certified by the National Bureau of Standards or with chromel-alumel thermocouples that had been calibrated against a certified Pt-Pt, 10% Rh thermocouple. With the certified Pt-Pt, 10% Rh thermocouples, an accuracy of at least $1^{o}C$ was attained, while the calibrated chromel-alumel thermocouples gave an accuracy of about $2^{o}C$. To protect the calibration of the thermocouples, the wires of each thermocouple were encased in alundum thermocouple tubes. This arrangement provided stress-free support for the termocouples while still allowing them to be accurately positioned within the inner heating coil. By using two notched alundum discs (refer to the section on the vacuum furnace), the three thermocouples could be spaced 120^{o} apart on a circle concentric with the absorption cell. One thermocouple measured the temperature at the center of the cell, and the other two thermocouples measured the temperatures at the ends of the cell. After passing out of the furnace through neoprene glands, the thermocouple wires were immersed in an ice bath to provide a reference junction at $0^{o}C$. The ice bath consisted of six glass tubes partly filled with mercury and submerged to within an inch of their tops in melting ice. One thermocouple wire and one copper extension wire were inserted into the cold mercury in each glass tube to complete the electrical path to the measuring circuit. This arrangement eliminated any temperature gradient between the two wires that might generate a parasitic thermal e.m.f.

To preserve the full accuracy of the thermocouples, the measuring circuit must possess a comparable precision. A number of precautions

were, therefore, taken to insure the maximum possible precision in the measuring circuit. First, all metallic circuit components were of pure copper to minimize any parasitic thermal e.m.f. Secondly, a lead storage battery of 120 ampere-hour capacity was used as the D.C. voltage source because the voltage of ordinary dry cells drifted with use. Thirdly, all voltages were standardized with a Weston Standard Cell certified by the National Bureau of Standards. The circuit also had to be sensitive enough to measure the thermocouple e.m.f. to the nearest microvolt, when the Pt-Pt, 10% Rh thermocouples were being used. A Rubicon potentiometer with a least count of 0.5μv was, therefore, employed along with an undamped galvanometer (0.15μv/ mm voltage sensitivity) as the null point indicator. Finally, considerable care had to be exercised when taking temperature readings. The lead storage battery had to be standardized before and after a set of readings to check for any voltage drift that may have occurred. Also the galvanometer zero had to be checked periodically for drift. In this regard, the system proved to be very stable because these drifts were never great enough to cause more than a 0.2^{o}C uncertainty in the temperature.

The Optical System:

The experiments reported in this investigation were performed with the following optical system. For the source of continuous radiation, a high pressure mercury arc lamp was used. This lamp consisted of a quartz water jacket enclosing a quartz capillary with tungsten electrodes at either end. The capillary contained a few droplets of

mercury and argon gas at 2 mm. of Hg pressure. When operating, the lamp produced a brilliant pseudo-continuum of pressure broadened mercury lines. Although the pseudo-continuum displayed some residual line structure, none of this structure interfered with any of the measurements reported here. The lamp with its ballast resistance was normally operated at 1 to 1.5 amperes and 500 to 1200 volts D.C. provided directly from a D.C. generator.

Light emitted by the lamp was gathered by a 20 cm. focal length lithium fluoride-quartz achromat and was rendered parallel. After passing through a quartz furnace window and two square apertures (5/8" x 5/8"), the parallel beam entered the absorption cell. From there, it proceeded through two more square apertures (5/8" x 5/8") which passed only the light that had traversed the cell. The parallel beam emerged from the furnace through a second quartz window and was rendered convergent by a 40 cm. focal length lithium fluoride-quartz achromat. A mirror then intercepted the beam and deflected it toward a third lens above the spectrograph slit. This lens was a 20 cm. focal length lithium fluoride-quartz achromat mounted on a micrometer screw. The lens focused a line image of the capillary on the plane of the slit, and the adjustment of the micrometer screw aligned this line image exactly along the slit. Light from an iron arc could be sent into the spectrograph by rotating a mirror into position behind the 40 cm. lens.

The spectrograph used in this investigation was the Rowland mount instrument located in room one of Bridge Laboratory on the California Institute of Technology campus. The instrument was mounted vertically

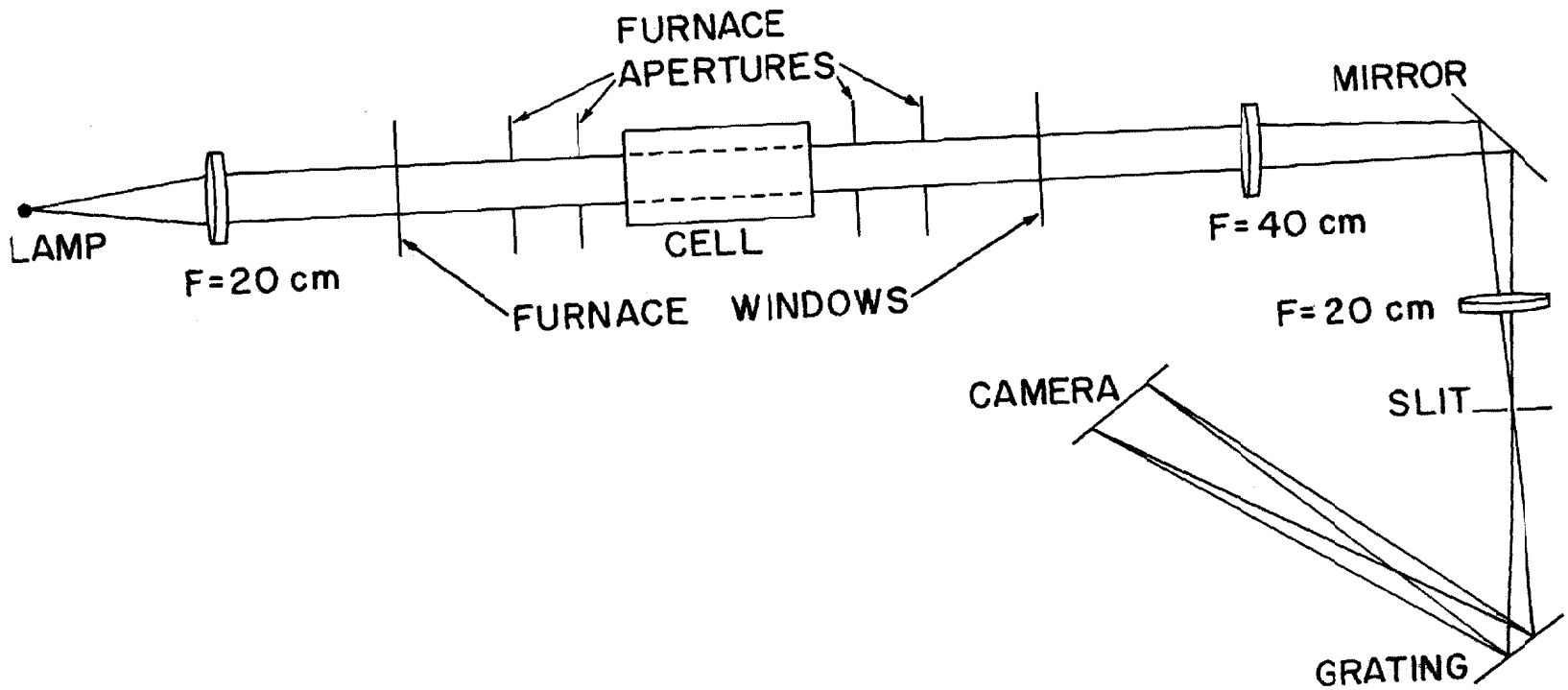

FIGURE II. THE OPTICAL SYSTEM

over a deep pit in the ground that provided adequate insulation for the grating against thermal disturbances and vibration. Essentially, the instrument consisted of a stationary slit, a grating holder capable of rotation and translation, and a movable camera mounted on rails. The motions of the camera and grating holder were coupled together so as to keep the slit, camera, and grating on the Rowland circle. Change of spectral region was accomplished by cranking the camera to the required position. Dispersion was provided by a concave Bausch and Lomb replica grating with the following specifications:

number of grooves per mm.	= 600/ mm.
width of ruling	= 5.5 in.
length of rulings	= 2.0 in.
concave radius	= 21 feet 10 in.
blaze wavelength (first order)	= 6000 Å.

Used with this spectrograph, the grating gave a first order dispersion of 2.504 Å/ mm. Since the spectrograph was always used in the second order, the actual linear dispersion realized in this investigation was 1.252 Å/ mm. Tests showed that 30μ was the proper slit width for this dispersion, and this was the slit width used. Finally, the band pass admitted into the spectrograph was limited by using a Corning red purple corex A filter (#7-54).

Photographic Photometry:

All the data reported here were photographed on Ilford N. 50 half-tone plates. These plates have very fine grain but only moderate speed. Typical exposure times were about 16 seconds. The fine grain

of this emulsion was a considerable advantage when weak lines were being scanned. Also these plates possessed sufficient contrast for the task of measuring weak lines. On the linear part of the characteristic curve, a change of 0.010 in the log intensity led to a 1% change in blackening. Since the Ilford plates possessed adequate contrast and speed as well as the fine grain, they were adopted for the photography in this investigation.

To be able to directly compare plates developed at different times, the photographic development process was rigidly standardized. All plates were developed for exactly four minutes in unused D-19 developer at 20°C. After development, the plates were fixed in hypo for 15 minutes, and then rinsed in tap water for two hours. Finally, the plates were rinsed in distilled water and then in alcohol. All handling of the plates was done with rubber gloves to prevent the oil on one's hands from staining the plates. When this procedure was faithfully followed, the plates always turned out very well — free of all dust, stains, and scratches.

All the plates taken in this investigation were calibrated with a step slit. The light from the high pressure mercury arc was used for the calibration plates since the tungsten ribbon lamp, normally used, was too slow. Although the mercury arc lamp did have occasional intensity fluctuations, the average length of these fluctuations was short compared with the exposure time. It was felt, therefore, that these fluctuations would average out during an exposure of 16 seconds. To make a calibration plate, the optical system was defocused until a one square inch area on the step slit was uniformly illuminated. The uniformity was checked by photographing the full astigmatic

image of one of the steps on the step slit. When this image was scanned on the microphotometer, the resulting trace on the chart showed that the middle third of the image was uniform to within 2%. Only this part of the image was used in making calibration plates. The calibration spectra were photographed through a step slit having twelve steps whose widths were accurately known. Since the intensity passing through such a step is proportional to the step width, $\Delta \log I$ was known for each step. In every case, the exposure time for a calibration plate was exactly equal to that of the plates being calibrated. After the calibration plates were developed, they were scanned on the microphotometer. The microphotometer results were then plotted against $\Delta \log I$ for the twelve steps to give the characteristic curve for the emulsion at the wavelength where it was used.

All the calibration curves obtained in this manner were plotted on a single large graph, and the values of log I were read off for every value of the transmission $T \geq 0.06$. The transmission is one minus the percent blackening. The resulting log I's were converted to intensities I on a relative scale. A graph was then plotted with I as the ordinate and T as the abscissa, and the resulting curve was traced over with silver conducting ink. Three such curves were drawn, one each for 3261 Å, 3281 Å and 3383 Å.

The photographic plates of spectral lines and the curves drawn in conducting ink were then taken to the photoelectric microphotometer in Robinson Laboratory. The plates were scanned in the normal way on the microphotometer. For weak lines, the plates were scanned twice to reduce the scatter due to photographic grain. Depending on

what line was being scanned, the proper curve drawn in conducting ink was inserted into a Moseley Autograf x-y recorder. While a plate was being scanned, the output of the microphotometer, which is proportional to the transmission T, was being fed into the input of the x-y recorder. This recorder had a curve follower, a small shuttle capable of two-dimensional motion anywhere in a plane. The curve follower would magnetically seek out the curve drawn in conducting ink and follow it. Since the input to the x-y recorder was proportional to T, the curve follower would automatically take up a position with the abscissa T. The output of the x-y recorder was proportional to the ordinate I of the curve follower. When the microphotometer was recording the transmission T, the x-y recorder would be producing an output proportional to I(T), the relative intensity corresponding to T. The output I(T) was then fed into a Leeds and Northrup Speedomax recorder. Thus, the recorder chart resulted in a plot of intensity I versus wavelength λ. For weak lines, the slowest speeds were used on both the recorder and microphotometer to give a wavelength scale factor of 3.65×10^{-2} Å (second order) per inch of chart. Once the weak lines were recorded on the chart, their areas were measured by the triangle approximation, and were then multiplied by the wavelength scale factor to give the corresponding equivalent width.

For strong lines measured in runs 1-CD, 2-CD, 1-AGL and 2-AGL, a somewhat different procedure was employed. The necessary emulsion calibration curves were first converted into potentiometer settings for the analog curve generator located in the microphotometer room of Robinson Laboratory. Essentially, the analog curve generator performed

the same function as the Moseley Autograf curve follower previously described: it electronically converted the transmission reading to an intensity reading so that an intensity versus wavelength plot resulted on the recorder chart. The resulting curves were then planimetered, and the areas obtained were multiplied by a wavelength scale factor to give the equivalent width. Depending on the magnitude of the spectral line, the wavelength scale factor was varied from 0.2193 Å (second order) per inch of chart to 3.5084 Å (second order) per inch of chart to give a convenient scale on the chart.

For strong lines measured in runs 1-AGR, 2-AGR, 1-PB, 1-ZN, 1-TLR, and 1-TLL, yet a third procedure was used. The necessary emulsion calibration curves were first put onto punched IBM computer cards in the form of a table of transmission versus log intensity. Next the photographic plates were scanned in the transmission mode on a microphotometer located at Wright-Patterson Air Force Base, Ohio. The resulting transmission versus wavelength curves were then converted into punched IBM cards by a Benson-Lehner Oscar Model F chart reader. On the card were recorded the transmission y, the wavelength coordinate x, and the spectral line identification. A computer program for an IBM 1620 was then written which performed the following functions First, the transmission of the base line was computed and then converted to the intensity I_o. Next, the transmission y(x) was converted by the computer program to the intensity I(x). Finally, the quantity $(I_o-I)/I_o$ was computed for the same value of the wavelength coordinate x. The computer then found the area under the curve by simply adding up all the $(I_o-I)/I_o$ values for every increment

Δx in the wavelength. The resulting areas were then multiplied by wavelength scale factors varying from 0.1253 Å (second order) per inch of chart to 6.265 Å (second order) per inch of chart to give the corresponding equivalent width.

IV. RESULTS AND CONCLUSIONS

In this section, the experimental results obtained in this investigation will be presented and compared with those of other investigators. Also the accuracy of the measurements will be discussed to establish an upper limit for the total experimental error. Finally, all the conclusions reached in this investigation will be presented here.

Estimation of Experimental Errors

This section will discuss the over-all precision in the data reported here. Generally, the precision attained will depend on the errors in the photographic photometry, the temperature measurements, and the published vapor pressures used to calculate the atomic density. Results obtained by photographic photometry can usually be relied upon to about ten per cent. Photometric errors result from grain noise in the emulsion or from uncertainties in the measurement of the transmission. For weak lines exposed on the linear portion of the emulsion calibration curve, grain noise is by far the dominant source of error. Its effect may be seen in the scatter shown in tables I, V, and VIII. In practice, a photometric accuracy for weak lines of about ten per cent has been routinely achieved as shown in the data for weak lines of Cd I λ3261 Å. On the other hand, the equivalent widths of strong lines rarely suffer from grain noise. Photometric uncertainties in strong lines generally arise from the difficulty in measuring transmissions less than 15% or greater than 85%. In almost all cases, a small part of the equivalent width came from outside the region of 15% to 85% transmission, and gave rise to some scatter in the data. However, inspection of the

equivalent widths reported here for strong lines indicates that this scatter did not exceed ten per cent in any case.

As stated previously, the experiments reported here are particularly vulnerable to errors in temperature measurement. Accordingly, every effort was made to exact the maximum accuracy from the temperature measurement. The entire temperature measuring circuit was constructed of copper to minimize parasitic thermal voltages, and its sensitivity was adjusted so that one microvolt (0.1° C) was clearly resolvable on the potentiometer. Also the thermocouples themselves were carefully calibrated against a standard thermocouple from the National Bureau of Standards. This calibration was carried out over the entire range of temperatures covered in this investigation. As a result of these precautions, it was possible to make thermocouple readings with an uncertainty not exceeding 1° C. An error of this magnitude in the temperature would cause only a 5% error in the atomic density for a weak line and only a 2% error in the atomic density for a strong line.

As in the case of the temperature measurements, an effort was made to secure reliable vapor pressure data from which to calculate atomic densities. Since the self-broadening cross sections depend on the square of the atomic density, it was important to select for study only those elements with accurately known vapor pressures. For this reason, Hultgren's [20] estimates of the uncertainties in the heats of vaporization of Ag, Cd, Pb, and Zn were used to verify that these elements possessed well-established vapor pressure curves. In each case, the maximum uncertainty in the heat of vaporization would yield an error

not exceeding 15%. For the element thallium, the vapor pressure measurements of Nesmeyanov were selected [21]. Using the latest state of the art techniques, Nesmeyanov and his co-workers measured the vapor pressure curve of thallium by both the Knudsen Effusion Method and the Langmuir Method, and obtained good agreement between both methods. Such agreement indicates that thallium also possesses a vapor pressure curve sufficiently well-established for use in cross section measurements.

Cd I, λ 3261

The cadmium line λ 3261 arises from the intersystem transition between the ground state ^1S_o and the state $^3P_1{}^o$, 3.78 e.v. above it. Vapor pressures for cadmium were obtained from a special compendium of thermodynamical properties of metals compiled by the Minerals Research Laboratory, University of California at Berkeley [20]. The table of cadmium vapor pressures in that book was calculated assuming that the heat of vaporization of cadmium at 298 °K was ΔH = 26,770 (± 150) cal/mole. This value represents the weighted average of the results of fourteen different investigators. Therefore, cadmium vapor pressures from this source can be considered among the most reliable values available at this time. The uncertainty in ΔH of 150 cal/mole would lead to a maximum error of 12% in the atomic density for the range of temperatures used. Equivalent widths W_λ were measured over a temperature range, 475.8 °K to 939.0 °K, corresponding to a range of atomic densities, 7.93×10^{12} atoms/cm^3 to 2.23×10^{18} atoms/cm^3. The equivalent widths ranged from 4.24×10^{-11} cm. to 4.35×10^{-8} cm.

For weak lines, fifty measurements of the equivalent width were averaged together at one temperature to give a final average: W_λ = 4.24×10^{-11} cm. Table I gives the information needed to calculate f. The W_λ reported in table I is the average of the five measurements taken from the same plate. Before using table I to obtain f, one must

Table I: Cd I, λ 3261: Data for Weak Lines

T = 475.8°K N = 7.93×10^{12} atoms/ cm^3

$\Delta\lambda_D$ = 2.885×10^{-11} cm. ℓ = 4.30 cm.

Run	$W_\lambda \times 10^{11}$ (cm.)	Run	$W_\lambda \times 10^{11}$ (cm.)
CD-4A	4.76	CD-6B	4.38
CD-4B	4.37	CD-7A	4.12
CD-5A	4.26	CD-7B	3.87
CD-5B	4.34	CD-8A	4.16
CD-6A	3.86	CD-8B	4.31

Average W_λ = 4.24×10^{-11} cm.

consider the fine structure of Cd I, λ 3261. The unresolved line recorded on the photographic plate contains all the components of the fine structure pattern. If the separation between the components is greater than the Doppler width $\Delta\lambda_D$, then the observed equivalent width should be treated as the sum of the equivalent widths of each unresolved fine structure component. For cadmium the number of components can be quite large since cadmium has eight stable isotopes. (See table II). Brix and Steudel [22] have measured the fine structure pattern of Cd I, λ 3261. According to them, the hyperfine structure

Table II: The Stable Isotopes of Cadmium

Isotope:	106	108	110	111	112	113	114	116
% Abundance:	1.22	0.88	12.39	12.75	24.21	12.26	28.86	7.58

pattern consists of three groups of components with the intensity ratios 2:9:1. The middle group contains the components due to the even isotopes 110, 112, and 114. The isotope effect splits this group into a band, 29.5 cm^{-1} (3.13×10^{-11} cm.) wide. Thus, most of the contribution to the equivalent width will come from this middle group. The Cd I, λ 3261 line may, therefore, be treated as single. Using the data in table I in equations II-57a and II-57b gives the average value:

$$\text{Cd I } \lambda 3261: \quad f = 1.94 \times 10^{-3} \tag{IV-1a}$$

$$\gamma_N = 4.03 \times 10^{5} \text{ (ang. sec.)}^{-1} \tag{IV-1b}$$

For strong lines, the equivalent width was measured at eighteen different temperatures in two separate runs, 1-CD and 2-CD. These two cadmium runs can be considered independent in that two different sets of thermocouples and two different absorption cells were used to obtain the data. Each value of W_λ reported in tables III and IV represents the average of fourteen measurements made at the same temperature. The procedure described at the very end of section II was used to reduce the data. It is interesting to note that the constant A came out to be zero in both runs, thus indicating that both runs were not contaminated to any measurable extent by a foreign gas.

Table III: Cd I, λ 3261.06A

Run	W_λ (cm.)	T (^oK)	N($cm.^{-3}$)	$fa\gamma = W_\lambda^2 / NF^*$	$fa\gamma = A + BN^*$	obs. / calc.
1-CD-8A	5.438×10^{-10}	697.3	3.265×10^{16}	2.414×10^5	2.616×10^5	0.9226
1-CD-1B	1.325×10^{-9}	739.5	8.429×10^{16}	5.551×10^5	6.754×10^5	0.8218
1-CD-2A	2.661×10^{-9}	771.2	1.602×10^{17}	1.178×10^6	1.284×10^6	0.9176
1-CD-3A	5.252×10^{-9}	805.6	3.029×10^{17}	2.427×10^6	2.427×10^6	1.000
1-CD-9A	9.908×10^{-9}	838.3	5.252×10^{17}	4.981×10^6	4.208×10^6	1.184
1-CD-10A	1.456×10^{-8}	863.1	7.745×10^{17}	7.294×10^6	6.206×10^6	1.175
1-CD-11A	1.961×10^{-8}	890.7	1.163×10^{18}	8.812×10^6	9.319×10^6	0.9456
1-CD-12A	2.954×10^{-8}	916.2	1.653×10^{18}	1.407×10^7	1.325×10^7	1.062

$F = 3.7524 \times 10^{-41}$ $cm.^5$ sec. (ℓ = 3.53 cm.) A = 0 B = 8.013×10^{-12} $cm.^3$ $sec.^{-1}$

*for the definition of the constants F, A, and B, refer to equations II-56, II-58 and II-59.

Table IV: Cd I, λ 3261.06 Å

Run	W_λ(cm.)	T($^\circ$K)	N(cm.$^{-3}$)	$fa\gamma = W_\lambda^2/NF^*$	$fa\gamma = A + BN^*$	obs./calc.
2-CD-1A	1.017×10^{-9}	721.8	5.742×10^{16}	4.279×10^5	4.328×10^5	0.9887
2-CD-2A	2.319×10^{-9}	759.2	1.265×10^{17}	1.010×10^6	9.535×10^5	1.059
2-CD-3A	3.693×10^{-9}	790.5	2.308×10^{17}	1.404×10^6	1.740×10^6	0.8069
2-CD-4A	7.201×10^{-9}	823.3	4.103×10^{17}	3.002×10^6	3.093×10^6	0.9707
2-CD-5A	1.354×10^{-8}	865.0	7.972×10^{17}	5.463×10^6	6.009×10^6	0.9091
2-CD-6A	2.428×10^{-8}	899.0	1.307×10^{18}	1.072×10^7	9.852×10^6	1.087
2-CD-7A	4.346×10^{-8}	939.0	2.225×10^{18}	2.017×10^7	1.677×10^7	1.202

$F = 4.2095 \times 10^{-41}$ cm.^{5} sec. ($\ell = 3.96$ cm.) $A = 0$ $B = 7.538 \times 10^{-12}$ cm.^{3} sec.$^{-1}$

*for the definition of the constants F, A, and B, refer to equations II-56, II-58, and II-59.

Ag I, λ 3383:

The silver line λ 3383 arises from the electric dipole transition between the ground state $^2S_{\frac{1}{2}}$ and the state $^2P_{\frac{1}{2}}^o$, 3.65 e.v. above it. Vapor pressures for silver were taken from the same source as for cadmium [20] . In this source, the vapor pressure tables for silver were based on the heat of vaporization at 298°K, $\Delta H = 68,100 \pm 300$ cal/ mole. This value is the weighted average of nine different investigations. Hence, the vapor pressures obtained from this source may be regarded as very reliable. The uncertainty in ΔH of 300 cal/ mole could lead to an error in the atomic density of at most 12% over the temperature range used. Equivalent widths for this transition were measured over the temperature range, 1002.0°K to 1599.0°K, corresponding to a range in atomic densities, 4.65×10^{10} atoms/ cm^3 to 5.66×10^{15} atoms/ cm^3. The equivalent widths ranged in value from 4.64×10^{-11} cm. to 0.706×10^{-8} cm.

For weak lines, the equivalent widths from 42 measurements at a single temperature were averaged together to give a final average: $W_\lambda = 4.64 \times 10^{-11}$ cm. Each W_λ reported in table V is the average of the seven measurements taken on the same plate. Before using table V to calculate f, the effect of fine structure on W_λ must be considered. Silver has two stable isotopes, Ag^{107} (51.4%) and Ag^{109} (48.6%). Jackson and Kuhn [23] have measured the fine structure pattern for both silver resonance lines. According to them, the hyperfine splitting due to nuclear spin predominates over the isotope effect. The total fine structure pattern is given in the following diagram:

Table V: Ag I, λ 3383: Data for Weak Lines

$T = 1002.0^{o}K$ $\quad N = 4.65 \times 10^{10}$ atoms/ cm^3

$\Delta\lambda_D = 4.434 \times 10^{-11}$ cm. $\quad \ell = 4.40$ cm.

Run	$W_\lambda \times 10^{11}$ (cm.)	Run	$W_\lambda \times 10^{11}$ (cm.)
AG-1L	4.17	AG-4L	4.97
AG-2L	4.20	AG-5L	4.79
AG-3L	5.13	AG-6L	4.57

average $W_\lambda = 4.64 \times 10^{-11}$ cm.

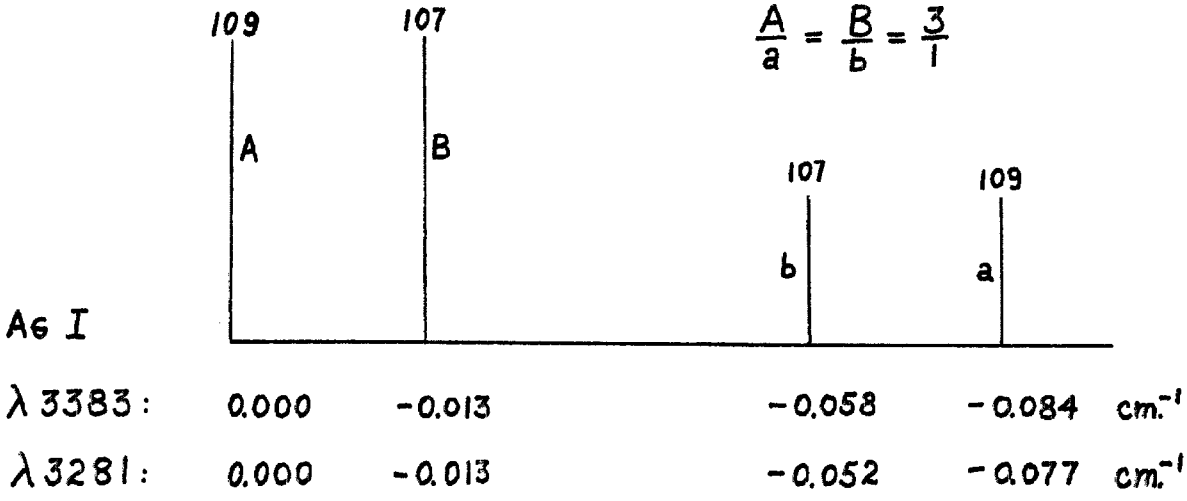

The diagram for Ag I, λ 3281 is also given here for later reference. While the isotope splitting is small, the nuclear hyperfine splitting is quite large, and actually exceeds 1.4 times the Doppler width $\Delta\lambda_D$. Thus, the equivalent width was divided into two parts in the ratio 3:1, and the value of C was separately computed for each part using II-57a. The resulting values of C were added together to form a new C which was inserted into II-57b to obtain f. The result was

Ag I λ3383: $f = 0.283$ (IV-2a)

$\gamma_N = 1.65 \times 10^8$ (ang. sec.)$^{-1}$ (IV-2b)

For strong lines, the equivalent width was measured at eighteen different temperatures in two separate runs, 1-AGL and 2-AGL. The letter L after the symbol for silver denotes the silver transition AG I λ3383 $\mathring{A}$. Each value of W_λ in tables VI and VII is the average of fourteen measurements taken at the same temperature. In analyzing the data in these two tables, the procedure described at the end of section II was employed. It is interesting to note from the data that run 2-AGL was contaminated by a small quantity of foreign gas, while run 1-AGL was free of any measurable contamination. Since the values of the constant B in both runs are in good agreement with one another, one may conclude that a small amount of foreign gas in the cell does not prevent a valid measurement of the self-broadening cross section. Also the absence of any Van der Waals broadening in run 1-AGL made it possible to get an independent measurement of the oscillator strength fa by inserting the constant A into equation II-59:

$$A = f_a \gamma_N = 0.47964 \times 10^8 \text{ (ang sec)}^{-1} \quad \text{(IV-3a)}$$

Ag I λ3383: $$\gamma_N = \frac{8\pi^2 r_o c}{\lambda^2}\left(\frac{g_l}{g_u}\right) f_a = 1.672 \times 10^8 \quad \text{(IV-3b)}$$

$$f_a = 0.287 \quad \text{(IV-3c)}$$

Comparison between equations IV-2 and equations IV-3 shows that very good agreement exists between the results obtained from weak lines and those from strong lines.

Table VI: Ag I, λ 3382.89 Å

Run	W_λ (cm.)	T($^\circ$K)	N(cm.$^{-3}$)	$fa\gamma = W_\lambda^2 / NF^*$	$fa\gamma = A + BN^*$	obs. / calc.
1-AGL-1A	5.702×10^{-10}	1333.3	1.302×10^{14}	4.569×10^{7}	5.078×10^{7}	0.8996
1-AGL-2A	7.713×10^{-10}	1364.5	2.196×10^{14}	4.957×10^{7}	5.272×10^{7}	0.9401
1-AGL-3A	1.023×10^{-9}	1401.2	3.942×10^{14}	4.857×10^{7}	5.650×10^{7}	0.8596
1-AGL-4A	1.545×10^{-9}	1444.1	7.513×10^{14}	5.813×10^{7}	6.424×10^{7}	0.9049
1-AGL-5A	2.594×10^{-9}	1484.8	1.338×10^{15}	9.201×10^{7}	7.695×10^{7}	1.196
1-AGL-6A	4.045×10^{-9}	1532.6	2.516×10^{15}	1.190×10^{8}	1.025×10^{8}	1.161
1-AGL-7A	7.063×10^{-9}	1599.0	5.660×10^{15}	1.613×10^{8}	1.706×10^{8}	0.9454

$F = 5.4655 \times 10^{-41}$ cm.^{5} sec. (ℓ = 4.44 cm.) $A = 4.796 \times 10^{7}$ sec^{-1} $B = 2.166 \times 10^{-8}$ cm.^{3} sec.$^{-1}$

*for the definition of the constants F, A, and B, refer to equations II-56, II-58, and II-59.

Table VII: Ag I, λ 3382.89 Å

Run	W_λ (cm.)	T($^\circ$K)	N(cm.$^{-3}$)	$fa\gamma = W_\lambda^2 / NF^*$	$fa\gamma = A + BN^*$	obs. / calc.
2-AGL-2A	7.601×10^{-10}	1327.5	1.178×10^{14}	9.838×10^{7}	8.983×10^{7}	1.095
2-AGL-3A	9.641×10^{-10}	1361.2	2.081×10^{14}	8.959×10^{7}	9.192×10^{7}	0.9747
2-AGL-4A	1.430×10^{-9}	1406.0	4.246×10^{14}	9.660×10^{7}	9.692×10^{7}	0.9967
2-AGL-5A	2.026×10^{-9}	1451.3	8.340×10^{14}	9.872×10^{7}	1.064×10^{8}	0.9281
2-AGL-6A	3.165×10^{-9}	1500.5	1.656×10^{15}	1.213×10^{8}	1.253×10^{8}	0.9680
2-AGL-7A	5.180×10^{-9}	1551.4	3.188×10^{15}	1.688×10^{8}	1.607×10^{8}	1.050
2-AGL-8A	7.700×10^{-9}	1597.7	5.573×10^{15}	2.134×10^{8}	2.158×10^{8}	0.9889

$F = 4.9854 \times 10^{-41}$ cm.^{5} sec. ($\ell = 4.05$ cm.) $A = 8.711 \times 10^{7}$ sec.$^{-1}$ $B = 2.309 \times 10^{-8}$ cm.^{3} sec.$^{-1}$

*for the definition of the constants F, A, and B, refer to equations II-56, II-58, and II-59.

Ag I, λ 3281:

The silver line λ 3281 arises from an electric dipole transition from the ground state $^2S_{\frac{1}{2}}$ to the state $^2P_{\frac{3}{2}}^o$, 3.76 e.v. above it. Since the data for the two silver resonance lines was taken simultaneously, the same range of atomic densities and temperatures will prevail here as for the other silver line. For weak lines, thirty-five measurements of the equivalent width, taken at the same temperature, were averaged together to obtain the final average: $W_\lambda = 7.22 \times 10^{-11}$ cm. Table VIII gives the pertinent data needed to calculate f. The

Table VIII: Ag I, λ 3281: Data for Weak Lines

T = 1002.0°K N = 4.65×10^{10} atoms/ cm^3

$\Delta\lambda_D = 4.301 \times 10^{-11}$ cm. $\ell = 4.04$ cm.

Run	$W_\lambda \times 10^{11}$ (cm.)	Run	$W_\lambda \times 10^{11}$ (cm.)
AG-1R	---	AG-4R	7.40
AG-2R	7.03	AG-5R	7.14
AG-3R	7.15	AG-6R	7.39

average $W_\lambda = 7.22 \times 10^{-11}$ cm.

fine structure pattern for this line was also measured by Jackson and Kuhn [23] . Their results are shown in the diagram in the preceding section. As before, the isotope splitting can be neglected, while the nuclear spin interaction separates the two components (A + B) and (a + b) by about 1.5 Doppler widths $\Delta\lambda_D$. Hence, the same method of calculating f must be used as for Ag I, λ 3383; that is, the constant C must be found separately for each component. The resulting values

of C must then be added together to obtain f from II-57b. When the calculation is performed this way, the result is:

$$\text{Ag I } \lambda 3281: \quad f = 0.524 \tag{IV-4a}$$

$$\gamma_N = 1.63 \times 10^8 \text{ (ang. sec.)}^{-1} \tag{IV-4b}$$

For strong lines, the equivalent width was measured at eighteen different temperatures in two separate runs, 1-AGR and 2-AGR. The letter R after the symbol for silver denotes the silver transition AG I $\lambda 3281$ Å. Each value of W_λ in tables IX and X is the average of seven measurements taken at the same temperature. The range of equivalent widths was from 8.16×10^{-10} cm to 1.03×10^{-8} cm. In analyzing the data in tables IX and X, the procedure described at the end of section II was employed. It is interesting to note from the data that run 2-AGR was contaminated by a small quantity of foreign gas, while run 1-AGR was free of any measurable contamination. Since the values of the constant B are in good agreement with one another, one may conclude that a small amount of foreign gas in the cell does not prevent one from validly measuring the self-broadening cross section. Also the absence of any Van der Waals broadening in run 1-AGR permitted an independent measurement of the oscillator strength fa. The constant A was inserted into equation II-59 with the result:

$$A = f_a \gamma_N = 0.99244 \times 10^8 \text{ (ang sec}^{-1}) \tag{IV-5a}$$

$$\text{Ag I } \lambda 3281: \quad \gamma_N = \frac{8\pi^2 r_o c}{\lambda^2} \left(\frac{g_\ell}{g_u} \right) f_a = 1.754 \times 10^8 \tag{IV-5b}$$

Table IX: Ag I, λ 3280.68 Å

Run	W_λ (cm.)	T(°K)	N(cm.$^{-3}$)	$fa\gamma = W_\lambda^2 / NF^*$	$fa\gamma = A + BN^*$	obs. / calc.
1-AGR-1A	8.157×10^{-10}	1333.3	1.302×10^{14}	1.057×10^{8}	1.052×10^{8}	1.004
1-AGR-2A	9.821×10^{-10}	1364.5	2.196×10^{14}	9.085×10^{7}	1.094×10^{8}	0.8308
1-AGR-3A	1.403×10^{-9}	1401.2	3.942×10^{14}	1.033×10^{8}	1.174×10^{8}	0.8798
1-AGR-4A	2.179×10^{-9}	1444.1	7.513×10^{14}	1.307×10^{8}	1.338×10^{8}	0.9767
1-AGR-5A	3.378×10^{-9}	1484.8	1.338×10^{15}	1.764×10^{8}	1.609×10^{8}	1.097
1-AGR-6A	5.552×10^{-9}	1532.6	2.516×10^{15}	2.534×10^{8}	2.151×10^{8}	1.178
1-AGR-7A	9.664×10^{-9}	1599.0	5.660×10^{15}	3.413×10^{8}	3.599×10^{8}	0.9483

$F = 4.8343 \times 10^{-41}$ cm.^{5} sec. ($\ell = 4.44$ cm.) $A = 9.924 \times 10^{7}$ sec.$^{-1}$ $B = 4.606 \times 10^{-8}$ cm.^{3} sec.$^{-1}$

*for the definition of the constants F, A, and B, refer to equations II-56, II-58, and II-59.

Table X: Ag I, λ 3280.68 Å

Run	W_λ (cm.)	T(°K)	N(cm.$^{-3}$)	$fa\gamma = W_\lambda^2 / NF^*$	$fa\gamma = A + BN^*$	obs. / calc.
2-AGR-2A	9.691×10^{-10}	1327.5	1.178×10^{14}	1.808×10^{8}	1.712×10^{8}	1.056
2-AGR-3A	1.302×10^{-9}	1361.2	2.081×10^{14}	1.847×10^{8}	1.755×10^{8}	1.052
2-AGR-4A	1.872×10^{-9}	1406.0	4.246×10^{14}	1.872×10^{8}	1.858×10^{8}	1.007
2-AGR-5A	2.680×10^{-9}	1451.3	8.340×10^{14}	1.953×10^{8}	2.054×10^{8}	0.9508
2-AGR-6A	4.067×10^{-9}	1500.5	1.656×10^{15}	2.265×10^{8}	2.446×10^{8}	0.9259
2-AGR-7A	6.730×10^{-9}	1551.4	3.188×10^{15}	3.222×10^{8}	3.177×10^{8}	1.014
2-AGR-8A	1.034×10^{-8}	1597.7	5.573×10^{15}	4.351×10^{8}	4.315×10^{8}	1.009

$F = 4.4097 \times 10^{-41}$ cm.^{5} sec. ($l = 4.05$ cm.) $A = 1.656 \times 10^{8}$ sec.$^{-1}$ $B = 4.770 \times 10^{-8}$ cm.^{3} sec.$^{-1}$

*for the definition of the constants F, A, and B, refer to equations II-56, II-58, and II-59.

$$f_a = 0.566 \qquad \text{(IV-5c)}$$

Comparison between equations IV-4 and IV-5 shows that very good agreement exists between the results obtained from weak lines and those from strong lines.

Zn I, λ 3076:

The zinc line λ 3076 arises from the intersystem transition between the ground state $^1S_0$ and the state $^3P_1{}^o$, 4.03 e.v. above it. Vapor pressures for zinc were taken from Hultgren's tables [20] . In this source, the vapor pressure tables for zinc were based on the heat of vaporization at 298°K, ΔH = 31, 215 $\pm$ 50 cal. / molc. This valuc is the weighted average of a number of different investigations and may be considered the most reliable value presently available. The uncertainty in ΔH of 50 cal. / mole could lead to an error in the atomic density of at most 5% over the temperature range used. Equivalent widths for this transition were measured over the temperature range 856. 5°K and 1163. 1°K, corresponding to a range of atomic densities, 8.99×10^{16} atoms/ cm^3 to 5.12×10^{18} atoms/ cm^3. The equivalent widths ranged in value from 3.63×10^{-10} cm to 2.00×10^{-8} cm. Each equivalent width reported in table XI is the average of seven measurements taken at the same temperature. In analyzing the data from table XI, the procedure described at the end of section II was employed. The reduction of the data was carried out using the oscillator strength obtained by the lifetime measurement of M. Dumont [24] .

$$\text{Zn I, } \lambda 3076 \quad f_a = 1.33 \times 10^{-4} \qquad \text{(IV-6)}$$

Table XI: Zn I, λ 3075.90 Å

Run	W_λ (cm.)	T(^oK)	N(cm^{-3})	$fa\gamma = W_\lambda^2 / NF^*$	$fa\gamma = A + BN^*$	obs. / calc.
1-ZN-1A	3.627×10^{-10}	856.5	8.990×10^{16}	4.688×10^4	Not Used	Not Used
1-ZN-2A	6.824×10^{-10}	894.9	1.768×10^{17}	8.438×10^4	6.954×10^4	1.213
1-ZN-3A	1.067×10^{-9}	935.4	3.359×10^{17}	1.086×10^5	1.321×10^5	0.8218
1-ZN-4A	1.887×10^{-9}	970.1	5.564×10^{17}	2.050×10^5	2.188×10^5	0.9368
1-ZN-5A	3.174×10^{-9}	1009.1	9.391×10^{17}	3.437×10^5	3.694×10^5	0.9304
1-ZN-6A	5.409×10^{-9}	1049.3	1.540×10^{18}	6.086×10^5	6.057×10^5	1.005
1-ZN-7A	8.047×10^{-9}	1086.5	2.352×10^{18}	8.820×10^5	9.251×10^5	0.9534
1-ZN-8A	1.331×10^{-8}	1124.7	3.516×10^{18}	1.615×10^6	1.383×10^6	1.168
1-ZN-9A	1.998×10^{-8}	1163.1	5.120×10^{18}	2.497×10^6	2.014×10^6	1.240

$F = 3.1215 \times 10^{-41}$ cm.^{5} sec. (ℓ = 3.71 cm.) A = 0 B = 3.933×10^{-13} cm.^{3} sec.$^{-1}$

*for the definition of the constants F, A, and B, refer to equations II-56, II-58, and II-59.

The results in table XI show that Van der Waals broadening is absent. However, the radiation damping width for this zinc transition is several orders of magnitude smaller than the self-broadening damping width at the lowest temperature measured. It was not possible, therefore, to measure the oscillator strength for this transition as was the case for silver.

Pb I, λ 2833:

The lead line λ 2833 arises from the electric dipole transition between the ground state $^3P_0$ and the state $^3P_1{}^o$, 4.38 e.v. above it. Vapor pressures for lead were taken from Hultgren's tables [20] . In this source, the vapor pressure tables for lead were based on the heat of vaporization at 298°K, $\Delta H = 46,000 \pm 300$ cal./mole. This value represents the weighted average a number of different investigations, and is probably the most reliable value presently available. The uncertainty in ΔH of 300 cal./mole could lead to an error in the atomic density of at most 15% over the temperature range used. Equivalent widths for this transition were measured over the temperature range, 982.4°K to 1473.8°K, corresponding to a range in atomic densities, 8.38×10^{13} atoms/cm^3 to 9.74×10^{16} atoms/cm^3. The equivalent widths ranged in value from 4.29×10^{-10} cm to 3.18×10^{-8} cm. Each equivalent width reported in table XII is the average of seven measurements taken at the same temperature. In analyzing the data from table XII, the procedure described at the end of section II was employed. The reduction of the data was carried out using the oscillator strength

Table XII: Pb I, λ 2833.07 Å

Run	W_λ (cm.)	T (°K)	N (cm.$^{-3}$)	$fa\gamma = W_\lambda^2 / NF^*$	$fa\gamma = A + BN^*$	obs. / calc.
1-PB-1A	4.285×10^{-10}	982.4	8.376×10^{13}	9.379×10^{7}	Not Used	Not Used
1-PB-2A	5.610×10^{-10}	1041.9	2.858×10^{14}	4.711×10^{7}	4.251×10^{7}	1.108
1-PB-3A	9.434×10^{-10}	1101.5	8.503×10^{14}	4.478×10^{7}	4.513×10^{7}	0.9923
1-PB-4A	1.410×10^{-9}	1155.4	2.065×10^{15}	4.119×10^{7}	5.075×10^{7}	0.8116
1-PB-5A	2.496×10^{-9}	1206.6	4.445×10^{15}	5.997×10^{7}	6.177×10^{7}	0.9708
1-PB-6A	4.793×10^{-9}	1267.4	1.011×10^{16}	9.722×10^{7}	8.799×10^{7}	1.105
1-PB-7A	8.975×10^{-9}	1328.5	2.138×10^{16}	1.612×10^{8}	1.402×10^{8}	1.150
1-PB-8A	1.619×10^{-8}	1395.6	4.498×10^{16}	2.494×10^{8}	2.494×10^{8}	1.000
1-PB-9A	3.179×10^{-8}	1473.8	9.742×10^{16}	4.437×10^{8}	4.921×10^{8}	0.9017

$F = 2.3373 \times 10^{-41}$ cm.^{5} sec. (ℓ = 3.86 cm.) $A = 4.119 \times 10^{7}$ sec.$^{-1}$ $B = 4.629 \times 10^{-9}$ cm.^{3} sec.$^{-1}$

*for the definition of the constants F, A, and B, refer to equations II-56, II-58, and II-59.

obtained by the atomic beam method by G. D. Bell and R. B. King [25] :

$$\text{Pb I, } \lambda 2833 \quad f_a = 0.23 \qquad \text{(IV-7)}$$

A Tesla coil revealed the presence of a small quantity of gas in the lead cell. Thus, no attempt was made to calculate the oscillator strength from the constant A.

Tl I, $\lambda 3776$:

The thallium line $\lambda 3776$ arises from the electric dipole transition between the ground state $^2P^o_{\frac{1}{2}}$ and the state $^2S_{\frac{1}{2}}$, 3.28 e.v. above it. Vapor pressures for thallium were taken from the tables of A. N. Nesmeyanov [21] , and were based on the heat of vaporization at 298°K, ΔH = 42,970 cal. / mole. Nesmeyanov and his co-workers measured the thallium vapor pressure curve by two independent and well-established methods: the Langmuir Method and the Knudsen Effusion Method. They obtained good agreement between the results of both methods, thus indicating that their vapor pressure measurements are of good quality. There is additional support to believe that Nesmeyanov's vapor pressure curve is the most reliable one presently available. The oscillator strength for the thallium transition $\lambda 3776$ is a well-established value. It was measured by Demtroder [26] whose lifetime measurement gave f_a = 0.128, by J. K. Link [27] who got f_a = 0.127 by the atomic beam method, and by G. S. Kvater [28] who obtained f_a = 0.125 by the hook method. Kvater's value was obtained from measurements of the quantity Nf_a which the hook

method is able to measure with a precision of about 4%. Later after Kvater's death, L. V. Gurvich [28] published Kvater's data, and reduced it to the absolute scale by using Nesmeyanov's vapor pressure curve. Gurvich obtained the value $f_a = 0.125 \pm 0.004$, quoted above, and thus showed that Nesmeyanov's vapor pressure curve was consistent with the oscillator strengths measured by Demtroder and Link. Since the latter two investigations did not use vapor pressure curves to obtain their oscillator strengths, the agreement of Gurvich's and Kvater's measurements with theirs establishes the reliability of Nesmeyanov's thallium vapor pressure curve. On the other hand, when Hultgren's [20] thallium vapor pressure curve is used along with Kvater's Nf_a values, the resulting oscillator strength is some 30% higher than those of Demtroder and Link. For these reasons therefore, Nesmeyanov's vapor pressures were chosen over those of Hultgren.

Equivalent widths for the thallium transition λ 3776 were measured over the temperature range, 975.2°K to 1330.1°K, corresponding to a range in atomic densities of 9.09×10^{14} atoms/ cm^3 to 1.81×10^{17} atoms/ cm^3. The equivalent widths ranged in value from 1.72×10^{-9} cm. to 8.69×10^{-8} cm. Each equivalent width reported in table XIII is the average of seven measurements taken at the same temperature. In analyzing the data from table XIII, the procedure described at the end of section II was employed. The reduction of the data was carried out using the oscillator strength obtained by the hook method by G. S. Kvater and L. V. Gurvich [28] :

Table XIII: Tl I λ 3775.72 Å

Run	W_λ (cm.)	T (^oK)	N ($cm.^{-3}$)	$fa\gamma = W_\lambda^2 / NF^*$	$fa\gamma = A + BN^*$	obs. / calc.
1-TLL-1A	1.717×10^{-9}	975.2	9.078×10^{14}	4.469×10^{7}	Not Used	Not Used
1-TLL-2A	3.052×10^{-9}	1035.4	2.926×10^{15}	4.385×10^{7}	Not Used	Not Used
1-TLL-3A	6.212×10^{-9}	1099.9	8.820×10^{15}	6.027×10^{7}	5.988×10^{7}	1.005
1-TLL-4A	1.280×10^{-8}	1152.3	1.971×10^{16}	1.145×10^{8}	1.100×10^{8}	1.041
1-TLL-5A	2.529×10^{-8}	1207.7	4.257×10^{16}	2.070×10^{8}	2.150×10^{8}	0.9625
1-TLL-6A	4.604×10^{-8}	1255.2	7.729×10^{16}	3.778×10^{8}	3.745×10^{8}	1.009
1-TLL-7A	8.693×10^{-8}	1330.1	1.809×10^{17}	5.754×10^{8}	Not Used	Not Used

$F = 7.2590 \times 10^{-41}$ $cm.^5$ sec. ($\ell = 3.80$ cm.) $A = 1.946 \times 10^{7}$ $sec.^{-1}$ $B = 4.594 \times 10^{-9}$ $cm.^3$ $sec.^{-1}$

*for the definition of the constants F, A, and B, refer to equations II-56, II-58, and II-59.

Tl I, λ 3776 $\quad f_a = 0.125$ (IV-8)

A Tesla coil revealed the presence of a small quantity of gas in the thallium cell. Thus no attempt was made to calculate the oscillator strength from the constant A. Also this thallium transition spans an unusually large fine structure interval [29] which was yet discernible in points 1-TLL-1A and 1-TLL-2A. These points were, therefore, not used in the least squares analysis to obtain the constants A and B. It should be pointed out also that the letter L after the symbol for thallium denotes the thallium transition λ 3776.

Tl I, λ 2768:

The thallium line λ 2768 arises from the electric dipole transition between the ground state $^2P_{\frac{1}{2}}^{o}$ and the state $^2D_{\frac{3}{2}}$, 4.48 e.v. above it. Vapor pressures for thallium were taken from Nesmeyanov's tables [21] as explained earlier. Since both thallium experiments utilized the same cell, the same range of temperatures and atomic densities prevailed as for the λ 3776 transition. The equivalent widths ranged in value from 1.27×10^{-9} cm to 8.52×10^{-8} cm. Each equivalent width reported in table XIV is the average of seven measurements taken at the same temperature. In analyzing the data from table XIV, the procedure described at the end of section II was employed. The reduction of the data was carried out using the oscillator strength obtained by the hook method by G. S. Kvater and L. V. Gurvich [28] :

Tl I, λ 2768 $\quad f_a = 0.272$ (IV-9)

Table XIV: Tl I, λ 2767.87 Å

Run	W_λ (cm.)	T(^oK)	N($cm.^{-3}$)	$fa\gamma = W_\lambda^2 / NF^*$	$fa\gamma = A + BN^*$	obs. / calc.
1-TLR-1A	1.267×10^{-9}	975.2	9.087×10^{14}	8.427×10^{7}	Not Used	Not Used
1-TLR-2A	2.437×10^{-9}	1035.4	2.926×10^{15}	9.682×10^{7}	Not Used	Not Used
1-TLR-3A	6.132×10^{-9}	1099.9	8.820×10^{15}	2.034×10^{8}	2.428×10^{8}	0.8377
1-TLR-4A	1.215×10^{-8}	1152.3	1.971×10^{16}	3.572×10^{8}	3.486×10^{8}	1.024
1-TLR-5A	2.365×10^{-8}	1207.7	4.257×10^{16}	6.270×10^{8}	5.709×10^{8}	1.098
1-TLR-6A	3.795×10^{-8}	1255.2	7.729×10^{16}	8.884×10^{8}	9.084×10^{8}	0.9780
1-TLR-7A	8.516×10^{-8}	1330.1	1.809×10^{17}	1.912×10^{9}	1.916×10^{9}	0.9982

$F = 2.0963 \times 10^{-41}$ $cm.^5$ sec. ($\ell = 3.80$ cm.) $A = 1.570 \times 10^{8}$ $sec.^{-1}$ $B = 9.722 \times 10^{-9}$ $cm.^3$ $sec.^{-1}$

*for the definition of the constants F, A, and B, refer to equations II-56, II-58, and II-59.

As stated earlier, gas was found in the thallium cell and thus the oscillator strength could not be calculated from the constant A. Also this transition in thallium spans a considerable fine structure interval which was yet discernible in points 1-TLR-1A and 1-TLR-2A. These points were, therefore, not used in the least squares analysis to obtain the constants A and B. It should be pointed out also that the letter R after the symbol for thallium denotes the thallium transition λ 2768.

Van der Waals Data:

As part of this investigation, the Van der Waals cross sections for cadmium and silver were also measured. These measurements were made to check if the presence of Van der Waals broadening affected in any way the measurement of the self-broadening cross sections reported here. In each case the foreign gas density was determined by admitting a known pressure of either CO_2 or H_2O vapor at 20°C. All the data needed to find the Van der Waals cross sections is given in table XV. For the cadmium data, each equivalent width represents the average of eighteen measurements taken at the same temperature, while for the silver data, each equivalent width is the average of seven measurements taken at the same temperature. In analyzing the data in table XV, equation II-56 was first squared, and Hultgren's vapor pressures [20] were used to obtain the total damping width $\gamma = \gamma_N + \gamma_W + \gamma_c$. The Van der Waals damping width γ_W was then found by subtracting the radiation damping width and the small resonance self-broadening width. The cross section

Table XV: Van der Waals Data for Cadmium and Silver

Transition	Gas	n^*	ℓ (cm.)	T (°K)	N^{**}	W_λ (cm.)	γ_W ($sec.^{-1}$)	σ ($cm.^2$)
Cd I, 3261	CO_2	1.729×10^{17}	4.04	688.1	2.602×10^{16}	1.422×10^{-9}	8.948×10^{8}	3.81×10^{-14}
Cd I, 3261	H_2O	1.647×10^{17}	4.99	693.1	2.944×10^{16}	1.257×10^{-9}	4.883×10^{8}	1.52×10^{-14}
Ag I, 3281	CO_2	1.746×10^{17}	3.86	1327.2	1.172×10^{14}	2.833×10^{-9}	2.694×10^{8}	8.14×10^{-14}
Ag I, 3383	CO_2	1.746×10^{17}	3.86	1327.2	1.172×10^{14}	1.648×10^{-9}	1.523×10^{8}	4.60×10^{-14}
Ag I, 3281	H_2O	1.647×10^{17}	3.40	1330.2	1.234×10^{14}	1.400×10^{-9}	5.724×10^{8}	1.29×10^{-14}
Ag I, 3383	H_2O	1.647×10^{17}	3.40	1330.2	1.234×10^{14}	1.177×10^{-9}	7.578×10^{8}	1.70×10^{-14}

*n is the foreign gas density in molecules/ cm^3.

**N is the atomic density in atoms/ cm^3.

for Van der Waals broadening was then found by using the relation:

$$\gamma_W = 2N \nu \sigma \qquad \text{(IV-10)}$$

where ν is the thermal relative velocity in cm/ sec., N is the foreign gas density in molecules/ cm^3, and σ is the Van der Waals cross section in cm^2.

Conclusions:

Of all oscillator strengths, perhaps the best established is the value for Cd I, λ 3261 Å. Several independent determinations of this oscillator strength have been made by a number of methods as indicated in table XVI [30] . From the agreement shown in table XVI, one may conclude that the oscillator strength reported here has an experimental uncertainty of approximately ten per cent and that any systematic errors present in the method of total absorption are probably below the detection limit. Table XVII shows that the oscillator strengths for the silver resonance lines were obtained in two independent experiments: from weak lines on the linear part of the curve of growth and also from strong lines on the square root portion of the curve of growth. In the first instance, the oscillator strength was obtained from equation II-57b where the dependence on N is linear, while in the latter case, the oscillator strength was obtained from equation II-56 when the resonance self-broadening term was negligible. In this latter case, the dependence on N was only as the square root. The agreement in table XVII, in view of the two different dependences on atomic density, implies that the silver vapor pressures used were highly accurate. Also table

XVII compares the relative oscillator strengths of both silver resonance lines measured by Filippov and Islamov [31] with those obtained in this investigation. Apparently, the results of both methods agree with one another when due allowance is made for the quoted experimental uncertainties.

Table XVI: Comparison of f-values for Cd I λ 3261 Å [30]

Investigator	Method	$f \times 10^3$
Kuhn	magneto-rotation	1.9 ± 0.2
Solcillct	magnetic depolarization	2.4
Ellett	magnetic depolarization	2.08
Filippov	hook*	1.8 ± 0.1
Koenig and Ellett	lifetime	1.9 ± 0.2
Soleillet	lifetime	1.95
King and Stockbarger	total absorption	2.3 ± 0.2
Webb and Messenger	lifetime	2.23 ± 0.07
Matland	lifetime	2.33 ± 0.06
Geneux and Wanders-Vincenz	lifetime	2.19 ± 0.07
Barrat and Butaux	magnetic resonance	2.12 ± 0.06
Byron and McDermott	mcthod not given	1.96
Lurio and Novick	method not given	1.96
This investigation [30]	total absorption	1.9 ± 0.2

mean value $f = 2.07 \times 10^{-3}$ standard deviation $\sigma = 0.18 \times 10^{-3}$

*Filippov, using the hook method, obtained $\frac{f(3261)}{f(2288)} = 1.5 \times 10^{-3} \pm 4\%$

This relative f-value can be reduced to an absolute scale by using f(2288) = 1.20 ± 0.05 measured by Kuhn and also by Zemansky.

Table XVII: Oscillator Strengths of the Silver Resonance Lines

Method	f(3281)	f(3383)	f(3281)/f(3383)
total absorption (weak lines)	0.524	0.283	1.85 ± 0.19
total absorption (strong lines)	0.566	0.287	1.97 ± 0.20
hook [31]			2.03 ± 0.06

For strong lines, further measurements were made to obtain cross sections for resonance self-broadening and for the Van der Waals broadening of the cadmium and silver lines. The Van der Waals measurements reported here were made primarily to test the validity of self-broadening cross sections obtained from cells contaminated by a small quantity (~ one mm. of Hg) of foreign gases. Independent mass spectrographic determinations revealed that these residual foreign gases were CO_2 and H_2O in the ratio of 2.45 (CO_2) to 1.00 (H_2O) at a total pressure of about one mm. of Hg. Reference to table XIX will show that the cross sections for self-broadening from runs 1AGR, 1AGL and 2AGR, 2AGL are in good agreement even though runs 2AGR, 2AGL were contaminated by foreign gases while runs 1AGR, 1AGL were uncontaminated. One may conclude therefore that the presence of a small amount of foreign gases will not affect the self-broadening cross sections measured in contaminated cells. The Van der Waals cross sections for the cadmium and silver lines are summarized in table XVIII. These cross sections, it can be seen, are sufficiently large to account for the additional broadening observed in runs 2AGR, 2AGL if a pressure of about one mm. of Hg is assumed. For this reason, no attempt was made to measure the

Table XVIII: Van der Waals Cross Sections for Cd and Ag

Transition	Foreign Gas	T(°K)	Cross Section σ (cm.^{2})	$\rho = \sqrt{\frac{\sigma}{\pi}}$ (Å)
Cd I λ3261	CO_2	688.1	3.81×10^{-14}	11.02
	H_2O	693.1	1.52×10^{-14}	6.97
Ag I λ3281	CO_2	1327.2	8.14×10^{-14}	16.09
	H_2O	1330.2	1.29×10^{-14}	6.40
Ag I λ3383	CO_2	1327.2	4.60×10^{-14}	12.10
	H_2O	1330.2	1.70×10^{-14}	7.37
Hg I λ2537 [32]*	CO_2		1.25×10^{-14}	
	H_2O		0.685×10^{-14}	

*Included in this table for sake of comparison.

radiation damping widths in any run where a Tesla coil revealed the presence of gas in the cell.

As mentioned earlier, the primary purpose of this investigation was to measure resonance self-broadening cross sections and to compare them with the theoretical predictions of equation II-52. Table XIX summarizes all the cross sections and the necessary data to analyze them. It is easily seen that the results reported here for $f_a \geq 0.1$ agree quite well with Foley's prediction when due allowance is made for the 20% precision of these measurements. Of particular importance is the scope of this test of Foley's theory. Five completely different spectral transitions were tested over a range of four in oscillator strengths and over a wave length range of 1.5. Also the range of thermal velocities in these measurements was almost a factor of two. Since all these ranges are well outside the 20% experimental uncertainty, it can be claimed that the resonance self-broadening cross section for

Table XIX: Final Results for Self-Broadening Cross Sections

Run	Transition	λ(Å)	f_a^*	f_e^{**}	B	$\gamma_{c/N} = B/f_a$	$\epsilon = \gamma_{c/N\lambda fe}$
1-ZN	$^1S_0 - {}^3P_1^\circ$	3075.90	1.33×10^{-4}	4.43×10^{-5}	3.933×10^{-13}	2.957×10^{-9}	2.170
1-CD	$^1S_0 - {}^3P_1^\circ$	3261.06	2.07×10^{-3}	6.90×10^{-4}	8.013×10^{-12}	3.871×10^{-9}	0.1720
2-CD	$^1S_0 - {}^3P_1^\circ$	3261.06	2.07×10^{-3}	6.90×10^{-4}	7.538×10^{-12}	3.641×10^{-9}	0.1618
1-AGR	$^2S_{1/2} - {}^2P_{3/2}^\circ$	3280.68	0.566	0.283	4.606×10^{-8}	8.137×10^{-8}	8.764×10^{-3}
2-AGR	$^2S_{1/2} - {}^2P_{3/2}^\circ$	3280.68	0.566	0.283	4.770×10^{-8}	8.428×10^{-8}	9.078×10^{-3}
1-AGL	$^2S_{1/2} - {}^2P_{1/2}^\circ$	3382.89	0.287	0.287	2.166×10^{-8}	7.547×10^{-8}	7.774×10^{-3}
2-AGL	$^2S_{1/2} - {}^2P_{1/2}^\circ$	3382.89	0.287	0.287	2.309×10^{-8}	8.044×10^{-8}	8.285×10^{-3}
1-PB	$^3P_0 - {}^3P_1^\circ$	2833.07	0.23	7.63×10^{-2}	4.629×10^{-9}	2.021×10^{-8}	9.350×10^{-3}
1-TLR	$^2P_{1/2}^\circ - {}^2D_{3/2}$	2767.87	0.272	0.136	9.722×10^{-9}	3.574×10^{-8}	9.495×10^{-3}
1-TLL	$^2P_{1/2}^\circ - {}^2S_{1/2}$	3775.72	0.125	0.125	4.594×10^{-9}	3.675×10^{-8}	7.787×10^{-3}

observed average $\epsilon = 8.648 \times 10^{-3}$ cm^2/ sec

Foley: $\epsilon = \frac{\pi}{3} r_o c = 8.846 \times 10^{-3}$ cm^2/ sec

*f_a = oscillator strength for absorption

**f_e = oscillator strength for emission

$f_a \geq 0.1$ depends linearly on the wavelength and the oscillator strength and is independent of the thermal velocity. Also the measurements reported here were made over a large range of atomic densities: over one order of magnitude for thallium extending to over three orders of magnitude for lead. Hence the results reported here do prove conclusively that the damping width for resonance self-broadening does depend linearly on the atomic density. In view of the scope of this test of Foley's predictions, it is felt that his theory of resonance self-broadening for transitions with oscillator strengths of order 1/10th has been substantially verified.

For spectral transitions with oscillator strengths much less than one, Foley predicts that self-broadening cross section should no longer depend linearly on the oscillator strength. The measurements for the cadmium and zinc transitions support this prediction since their cross sections differ by a factor of two whereas their oscillator strengths differ by almost a factor of sixteen (see table XIX). Such a large discrepancy is completely outside the 20% precision of the measurements. Foley's theory also predicts that in the impact approximation, the zinc and cadmium self-broadening damping widths should be linearly proportional to the atomic density and should have a velocity dependence of $v^{0.6}$. The large range of atomic densities covered in the zinc and cadmium runs clearly indicates that even in the limit of small oscillator strengths, the self-broadening damping width is linearly dependent on N. Unfortunately, the range of temperatures covered within the zinc and cadmium runs was too small

to accurately confirm the $V^{0.6}$ velocity dependence in the damping widths.

Lastly, it should be pointed out that the particular form of the method of total absorption used in this investigation possesses certain advantages for the measurement of oscillator strengths. As shown in the silver runs 1AGR and 1AGL, the quantity A in equation II-59 provides a measure of f_a^2 in the absence of any Van der Waals broadening, $\gamma_W = 0$. Obtaining oscillator strengths from II-59 has the following advantages not possessed by the method of total absorption applied to weak lines. First, the equivalent widths are quite large and are thus easier to measure with good precision and with almost complete freedom from the grain noise of the emulsion. Secondly, the temperatures required for strong lines are a good deal higher than those required for weak lines. Since the vapor pressures of all elements vary much more steeply, the lower the temperature, accuracy in measuring the temperature for strong lines is not nearly as critical as it is for weak lines. Thirdly, if the self-broadening damping is yet small compared with the radiation damping, the oscillator strength f_a depends on the square root of the atomic density N, and thus vapor pressure errors are reduced by at least a factor of two over the weak line case. Furthermore, now that Foley's theory of self-broadening has been verified for large oscillator strengths, it should be possible to measure f_a directly from resonance self-broadening cross sections. Such measurements would be far simpler to make than the corresponding weak line measurements although the precision would not be as good

due to the W_λ^2 dependence of the cross sections. Finally, it should be pointed out that oscillator strength measurements gotten from strong lines do not suffer normally from the uncertainty introduced by unresolved fine structure in weak lines.

Appendix I: The Validity of the Impact Approximation

In calculating the line shape for collision broadening, the impact or phase shift approximation was used. Essentially, this approximation assumes that the collisions are binary and that the duration of the collisions is very short compared with the lifetime of the absorption process [33]. The latter condition is particularly important since it permits replacing the collision integral II-21 with the sum of the individual phase shifts occurring in the time interval from 0 to t. Also the vanishingly small collision duration enables II-18 to be used in calculating the individual phase shift. However, the contour of a resonance self-broadened line could be equally well calculated using the statistical or static approximation. In this approximation, the collsion duration is assumed to be long compared with the liftime of the absorption process and/or the collisions are no longer binary. Either condition allows one to replace the effect of the collisions with an average portential acting over an entire radiation lifetime. Therefore, some justification should be given for employing the impact approximation in deriving the collision broadened line shape.

Essentially, the problem consists in selecting a suitable criterion for determining which approximation is applicable. If the parameters measured in the experiments are substituted into this criterion, then the proper approximation can be selected. From the foregoing discussion, the two approximations apparently differ from each other in their assumption about the duration of a collision compared with the radiation lifetime. Therefore, it seems reasonable to select as the

proper criterion the ratio of the collision duration τ_d to the radiation lifetime τ_R [33] ; that is,

$$\chi = \tau_d / \tau_R$$

If $\chi << 1$, then the impact approximation is valid; and conversely for $\chi >> 1$, the statistical approximation is valid.

The duration of a collision can be found by noting that the resonance self-broadening interaction falls to 1/8th of its maximum value when the distance between colliding atoms doubles. Thus,

$$\tau_d = \frac{2\rho}{\nu}$$

where $\nu = 2\sqrt{\frac{2RT}{\pi M}}$ is the mean velocity of the atoms and ρ is the distance of closest approach in a collision. A value for ρ can be obtained from the measured value of the resonance self-broadening width γ_c, by using the relation:

$$\gamma_c = 2N\nu(\pi\rho^2),$$

where N is the known atomic density. For the radiation lifetime, the values measured in the experiments reported here will be used. Hence, the ratio χ can be completely evaluated from experimentally measured quantities. Table XX shows the pertinent data needed to calculate χ. The values of χ shown in table XX are the maximum values attained in the experiments reported here. One may therefore conclude that the impact approximation is valid for the range of velocities and collision parameters encountered in this investigation.

Table XX: Calculation of the Ratio χ

Run	ν (cm./sec.)	ρ (cm.	τ_d (sec.)	τ_R (sec.)	χ
1-CD	4.21×10^{4}	12.2×10^{-8}	5.78×10^{-12}	1.47×10^{-10}	3.93×10^{-2}
2-CD	4.21	11.7	5.58	1.03	5.44
1-AGL	5.60	46.3	16.43	17.80	0.92
1-AGR	5.60	48.1	17.16	16.58	1.04
2-AGL	5.60	47.8	17.06	13.45	1.27
2-AGR	5.60	48.9	17.47	13.01	1.34
1-ZN	6.14	8.8	2.85	0.53	5.36
1-PB	3.88	28.8	14.84	51.61	2.88
1-TLL	3.71	39.7	21.38	21.72	9.84
1-TLR	3.71	39.2	21.09	14.22	14.83

Appendix II: Coordinate System for a Typical Atomic Collision

In Figure III, V is the velocity of atom 2, and the y and η axes are chosen to be parallel to this velocity. Similarly, the z and ζ axes and the x and ξ axes are parallel to one another. The parameter ρ is the distance of closest approach in the collision.

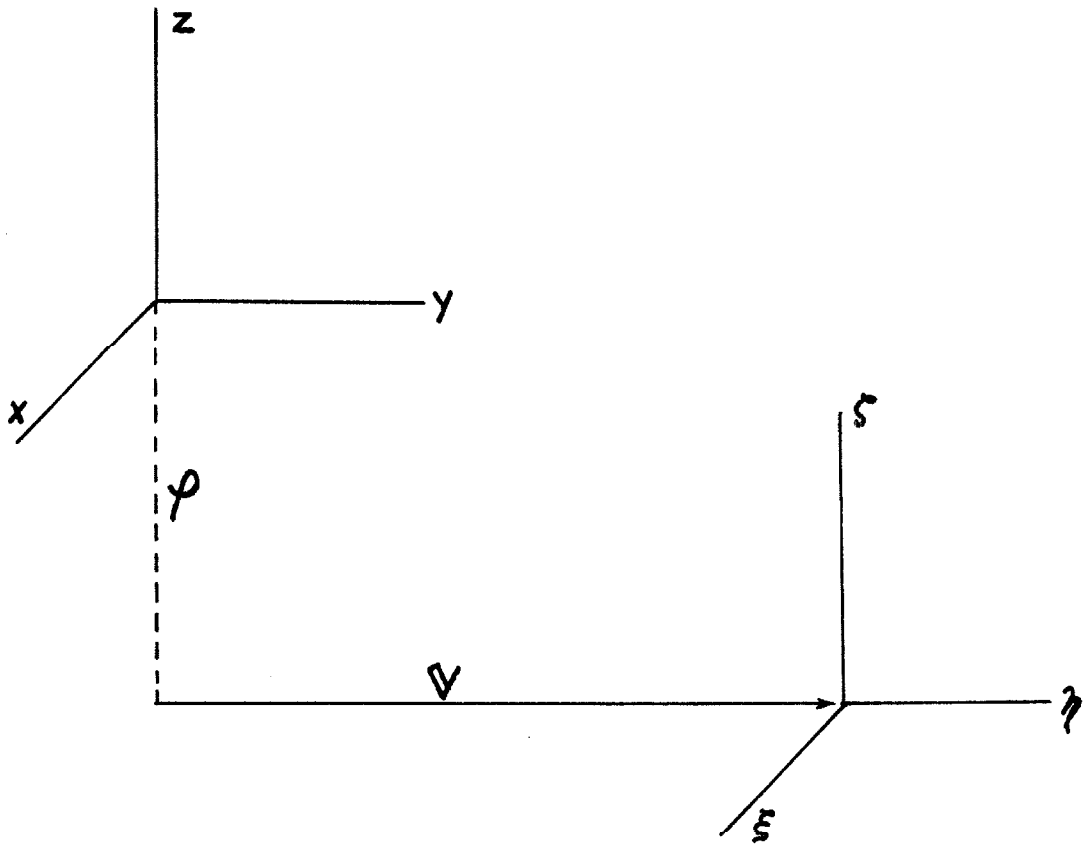

Figure III: Coordinate System for an Atomic Collision

REFERENCES

1. Breene, R. G., The Shift and Shape of Spectral Lines, Pergamon Press, New York (1961)
2. Byron, F. W., and Foley, H. M., Phys. Rev., 134, A625 (1964)
3. Weisskopf, V. F., Physikalische Zeitschrift, 34, 1 (1933)
4. Lindholm, E., Ark. Mat. Astron. Fys., 32A, No. 17 (1945)
5. Rozhdestwensky, D. S., and Penkin, N. P., Academy of Sciences USSR - Journal of Physics, 5, 319 (1941)
6. King, R. B., and Stockbarger, D. C., Ap. J., 91, 488 (1940)
7. Estabrook, F. G., Ap. J., 113, 684 (1950)
8. Unsold, A., Physik der Sterneatmospharen, p. 151, Springer, Berlin (1938)
9. Ladenberg, R., and Reiche, F., Ann. der Physik, 42, 181 (1913)
10. Bethe, H., and Salpeter, E., Quantum Mechanics of One and Two-Electron Systems, pp. 250, 256, Springer, Berlin (1957)
11. Panofsky, W., and Phillips, M., Classical Electricity and Magnetism, pp. 314, 317, and 322, Addison-Wesley, Boston (1956)
12. Weisskopf, V., and Wigner, E., Z. Physik, 63, 54 (1930) and 65, 18 (1931)
13. Hoyt, F., Phys. Rev., 36, 860 (1931)
14. Traving, G., Uber die Theorie der Druckverbreiterung von Spektrallinien, pp. 10-15, Braun Verlag, Karlsruhe (1960)
15. Mizushima, M., Phys. Rev., 83, 1061 (1951)

16. ter Haar, D., Elements of Statistical Mechanics, pp. 126 and 379, Rinehart, New York (1954)

17. Present, R. D., Kinetic Theory of Gases, p. 144, McGraw-Hill, New York (1958)

18. Condon, E. V., and Shortley, G. H., The Theory of Atomic Spectra, Cambridge University Press, New York (1957)

19. Unsold, A., Physik der Sterneatmospharen, p. 290, Springer, Berlin (1948)

20. Hultgren, R. (editor), Selected Values of Thermodynamic Properties of Metals and Alloys, pp. 28, 63, 207, 290, and 320, John Wiley & Sons, Inc., New York (1963)

21. Nesmeyanov, A. N., Vapor Pressure of the Chemical Elements, p. 245, Elsevier, Amsterdam (1963)

22. Brix, P., and Steudel, A., Z. Physik, 128, 260 (1950)

23. Jackson, D. A., and Kuhn, H., Proc. Roy. Soc. London, 158A, 372 (1937)

24. Dumont, M., Thèse de Troisième Cycle, Ecole Normale Supérieur, Paris (1962), (unpublished)

25. Bell, G. D., and King, R. B., Ap. J., 133, 718 (1961)

26. Demtroder, W., Z. Physik, 166, 42 (1962)

27. Lawrence, G. M., et al., Ap. J., 141, 293 (1965)

28. Gurvich, L. V., Optika i Spektros., 5, 205 (1958)

29. Landolt-Bornstein, Zahlenwerte und Funktionen, Vol. 1, No. 5, pp. 1-63, Springer-Verlag, Berlin (1952)

30. Bieniewski, T. M., M. N. R. A. S., 127, 365 (1964)

31. Islamov, I. I., and Filippov, A. N., Zh. Eksper. i Teor. Fiz., 3, 524 (1933)

32. Mitchell, A. C. G., and Zemansky, M. W., Resonance Radiation and Excited Atoms, p. 171, Cambridge University Press, London (1961)

33. Foley, H. M., Phys. Rev., 69, 620 (1946)